in vitro restimulated cells were collected and their OVA-specific cytotoxicity was measured by the following procedure.

CTL assay

For the CTL assay, freshly isolated IELs, SCs, or TILs were used. Cytolytic activity was measured using a standard ^{51}Cr-release assay as previously described (12). In brief, various numbers of effector cells were incubated with 3×10^3 ^{51}Cr-labeled targets for 6 h at 37°C in 200 μl of RPMI 1640 medium containing 10% FCS in round-bottom 96-well cell culture plates (BD Biosciences). After incubation, the plates were centrifuged for 10 min at $330 \times g$, and 100 μl of cell-free supernatants were collected to measure radioactivity with a Packard Auto-Gamma 5650 counter (Hewlett-Packard Japan). Maximum release was determined from the supernatant of cells that had been lysed by the addition of 5% Triton X-100, and spontaneous release was determined from target cells incubated without added effector cells. The percentage of specific lysis was calculated as 100 × (experimental release − spontaneous release)/(maximum release − spontaneous release). SEs of the means of triplicate cultures were always <5% of the mean. Each experiment was performed at least three times.

Measurement of in vivo antitumor effects

E.G7-OVA cells (5×10^6), OVA gene-transfected EL4 thymoma cells (19, 20), were implanted into the gastric or dermal tissue of syngeneic C57BL/6 mice (H-2^b). For tumor implantation into the gastric tissue, mice were anesthetized and underwent an abdominal operation and then E.G7-OVA cells in 50 μl of RPMI 1640 were injected into the muscle layer of the stomach using a syringe with a 29-gauge needle (Terumo). For implantation into the dermal tissue, mice were anesthetized and E.G7-OVA cells in
AQ: H 100 μl of RPMI 1640 were injected intradermally by a 29-gauge needle syringe. On day 3 after implantation into the gastric or dermal tissue, when the tumor mass became visible, tumor-bearing mice were orally or systemically administered OVA plus CT as described above. Seven days after the first administration, some of the mice were similarly boosted with the same materials. The growing tumors implanted into the gastric or dermal tissues were followed by measuring the length (a) and width (b), the and tumor volume (V) was calculated according to the formula $V = ab^2/2$ as reported previously (28). When the longer axis of each tumor was >20 mm, all mice were anesthetized and sacrificed according to the guidelines for the care and use of laboratory animals set by the NIH.

Histological analysis of tumor tissues

Freshly excised tumor tissues were embedded in Tissue-Tek OCT compound (Sakura Finetek) at −80°C. Tissue segments were sectioned at 6 μm using a cryostat. Sections were placed on a poly-L-lysine-coated glass slide, air dried, and then fixed in 10% formalin PBS for 5 min and stained with H&E. For immunohistochemical staining, sections were fixed in cold acetone for 5 min and incubated with blocking solution (Block-ace; Dainippon Pharmaceutical) for 30 min at 37°C and then incubated with biotin-conjugated rat anti-CD8β Ab (Caltag Laboratories) or control isotype-matched rat IgG2a Ab (Caltag Laboratories) overnight at 4°C. Endogenous peroxidase was quenched by incubation in 0.3% H_2O_2 and 0.1% NaN_3 in distilled water for 10 min. The sections were incubated with avidin-biotin peroxide complexes (Vectastain ABC kit; Vector Laboratories) followed by color reaction with a Vectastain diaminobenzidine substrate kit (Vector Laboratories).

Statistical analysis

Student's t test was used to determine the statistical significance of differences between groups in tumor growth. Data were considered significant at $p < 0.05$.

Results

Priming of OVA-specific CD8αβ-positive CTLs with direct cytotoxicity via oral administration with OVA plus CT

It has been reported that OVA-specific CTLs could be primed in C57BL/6 mice by oral or i.v. immunization with OVA plus CT together with nontoxic CTB, and specific cytotoxic activity was detected from immune SCs only when they were restimulated in vitro with irradiated OVA-expressing syngeneic tumor (E.G7-OVA) cells (18). It has also been shown that activated CTLs but not naive primed CTLs could represent antitumor responses in vivo (22). Similarly, we have recently observed in HIV-1-specific CTL-TCR transgenic mice that activated CTLs but not freshly isolated TCR-bearing CD8αβ-positive T cells showed specific cytotoxicity, and the most critical sites for activating TCR-bearing CD8αβ T cells were mucosal compartments when Tg mice were administered a specific Ag for TCR (12).

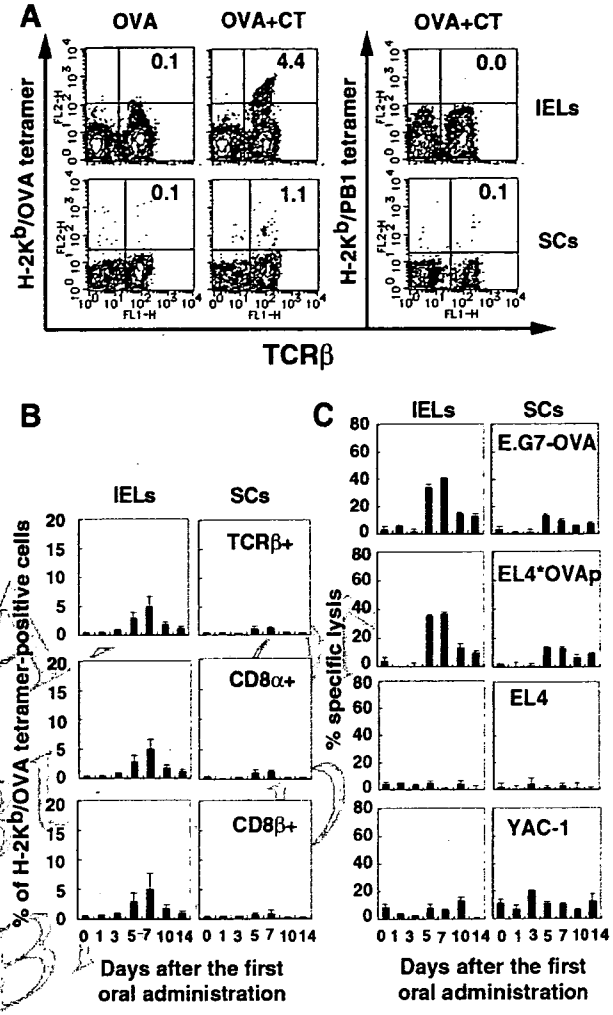

FIGURE 1. Analysis of OVA-specific direct cytotoxicities in IELs and SCs after primary immunization with OVA plus CT. *A*, Analysis of H-2K^b/OVA tetramer-positive cells. C57BL/6 mice were orally administered OVA or OVA plus CT once. IELs and SCs were collected from mice 5 days after the first oral administration, stained with either PE-labeled H-2K^b/OVA tetramer-SIINFEKL or H-2K^b/PB1 tetramer-SSYRRPVGI together with FITC-labeled anti-mouse TCRβ, and analyzed by flow cytometry. Each value represents the percentage of cells expressing both indicated markers. Data are representative of three independent experiments. *B*, Kinetics of H-2K^b/OVA tetramer-positive cells after primary immunization. C57BL/6 mice were orally administered OVA plus CT once. IELs and SCs were collected from mice at various days after the first oral administration, stained with PE-labeled H-2K^b/OVA tetramer together with FITC-labeled anti-mouse TCRβ, CD8α, or CD8β, and analyzed by flow cytometry. The results are shown as the mean ± SD of four mice. *C*, Kinetics of OVA-specific direct cytotoxic responses. C57BL/6 mice were orally primed and cells were collected as described in *B*. OVA-specific CTL responses were measured by ^{51}Cr-release assay using E.G7-OVA cells (H-2^b), YAC-1 cells, and EL4 cells (H-2^b) pulsed with or without 4 μM OVA-peptide, SIINFEKL, as target cells. E:T ratio was 100:1. The results shown as the mean ± SD in triplicate of pooled cells from two mice are representative of three independent experiments.

These findings prompted us to examine whether direct OVA-specific cytotoxic activity could be induced among IELs in mice AQ: I

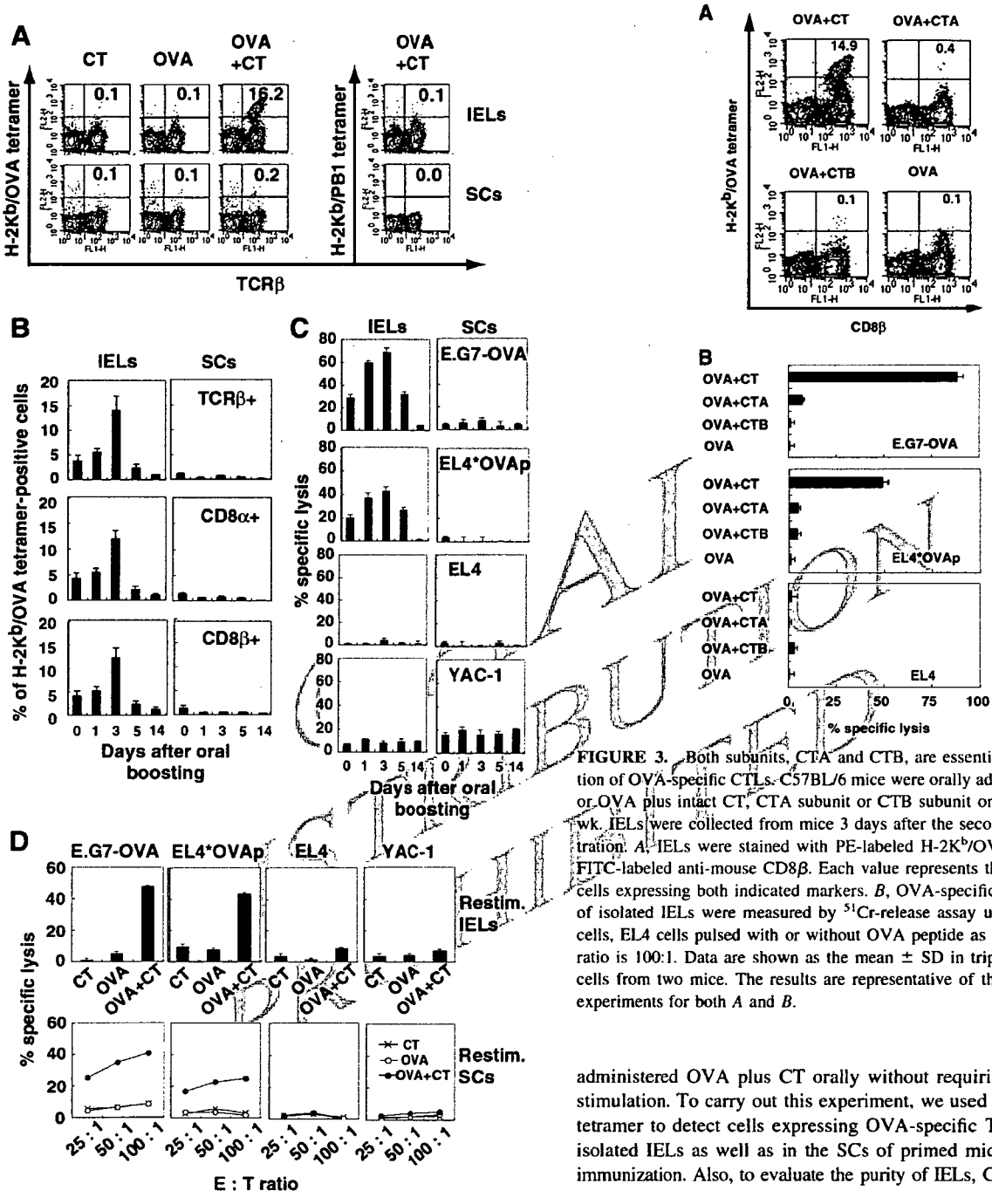

FIGURE 2. Expansion of direct OVA-specific cytotoxicities after oral boosting with OVA plus CT. *A*, Activated H-2K^b/OVA tetramer-positive cells after oral boosting. C57BL/6 mice were orally administered CT, OVA, or OVA plus CT once weekly for 2 wk. IELs and SCs were collected from mice 3 days after the second oral boost and stained with PE-labeled H-2K^b/OVA tetramer or H-2K^b/PB1 tetramer together with FITC-labeled anti-mouse TCRβ. Each value represents the percentage of cells expressing both indicated markers. Data are representative of three independent experiments. *B*, Kinetics of H-2K^b/OVA tetramer-positive cells after oral boosting. C57BL/6 mice were orally administered OVA plus CT once weekly for 2 wk. IELs and SCs were collected from mice at various days after the second oral boost, stained with PE-labeled H-2K^b/OVA tetramer together with FITC-labeled anti-mouse TCRβ, CD8α, or CD8β, and analyzed by flow cytometry. The results are shown as the mean ± SD of four mice. *C*, Kinetics of the secondary expansion of OVA-specific direct CTL responses. C57BL/6 mice were treated orally and the cells were collected as described in *B*. OVA-specific CTL responses were measured by ^{51}Cr-release assay using E.G7-OVA cells, YAC-1 cells, and EL4 cells pulsed with or without OVA peptide as targets. The E:T ratio is 100:1. The results shown as the mean ± SD in triplicate of pooled cells from two mice are representative of three independent experiments. *D*, Activation of OVA-specific CTLs by in vitro restimulation (Restim.). C57BL/6 mice were orally administered CT, OVA, or OVA plus CT once weekly for 2 wk. IELs (3×10^7) and SCs (3×10^7) were collected from mice 9 days after the second oral boost, and cocultured with 3×10^6 irradiated E.G7-OVA. Six days later, OVA-specific lysis of stimulated IELs and SCs was measured by ^{51}Cr-release assay. The E:T ratio is 100:1 in IELs and 100:1, 50:1, or 25:1 in SCs. The results are shown as the mean ± SD in IELs or the mean in SCs in triplicate of pooled cells from two mice. Data are representative of three independent experiments.

FIGURE 3. Both subunits, CTA and CTB, are essential for the induction of OVA-specific CTLs. C57BL/6 mice were orally administered OVA or OVA plus intact CT, CTA subunit or CTB subunit once weekly for 2 wk. IELs were collected from mice 3 days after the second oral administration. *A*, IELs were stained with PE-labeled H-2K^b/OVA tetramer and FITC-labeled anti-mouse CD8β. Each value represents the percentage of cells expressing both indicated markers. *B*, OVA-specific CTL responses of isolated IELs were measured by ^{51}Cr-release assay using E.G7-OVA cells, EL4 cells pulsed with or without OVA peptide as targets. The E:T ratio is 100:1. Data are shown as the mean ± SD in triplicate of pooled cells from two mice. The results are representative of three independent experiments for both *A* and *B*.

AQ: P

administered OVA plus CT orally without requiring in vitro restimulation. To carry out this experiment, we used a H-2K^b/OVA tetramer to detect cells expressing OVA-specific TCR in freshly isolated IELs as well as in the SCs of primed mice 5 days after immunization. Also, to evaluate the purity of IELs, CD103 (integrin

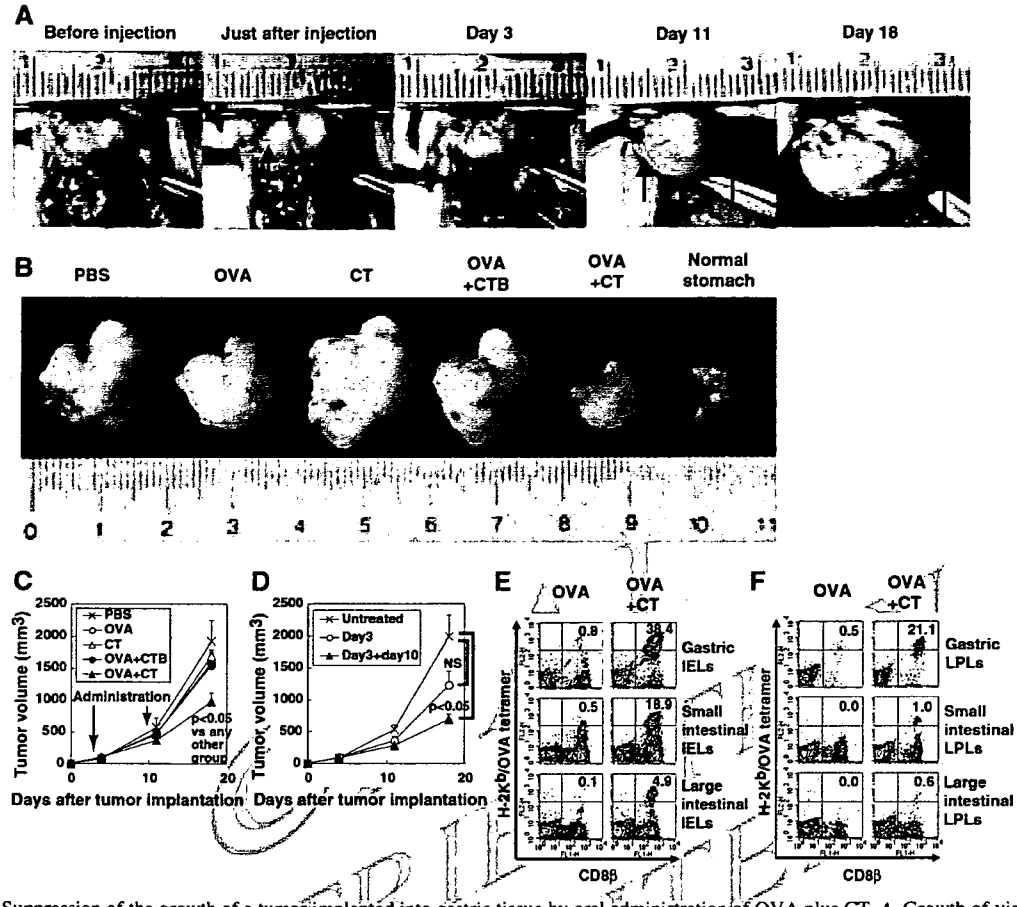

FIGURE 4. Suppression of the growth of a tumor implanted into gastric tissue by oral administration of OVA plus CT. *A*, Growth of visible tumor after implantation of E.G7-OVA cells into gastric tissue. C57BL/6 mice were implanted with 5×10^6 E.G7-OVA cells into the muscle layer of the stomach. Each day, the same mice were anesthetized and underwent an abdominal operation, and tumors were observed. Arrows point to both ends of the longer axis in the tumor. *B*, C57BL/6 mice were implanted with 5×10^6 E.G7-OVA cells into the muscle layer of the stomach. Three days later, tumor-bearing mice were orally administered PBS, OVA, CT, OVA plus CTB subunit, or OVA plus CT. Seven days later, the second oral administration was performed in the same manner. Stomachs were excised from the mice 18 days after tumor implantation, as well as from untreated, normal mice. *C*, Tumor volumes were calculated based on the formula described in *Materials and Methods*, and the results are shown as the mean ± SEM. The results were obtained from 9–13 mice per group. $p < 0.05$ indicates statistically significant difference between OVA plus CT (▲) and any other groups. *D*, C57BL/6 mice were implanted with E.G7-OVA cells in the stomach. Three days later, tumor-bearing mice were orally administered OVA plus CT or left untreated. Seven days later, some orally immunized mice were boosted in the same manner or left untreated. The results are shown as the mean ± SEM of 5–7 mice per group. $p < 0.05$ and NS indicate statistically significant and not significant differences, respectively, between the boosted (▲) and nonboosted (○) groups and the untreated group (×). *E* and *F*, Induction of CD8β and H-2K^b/OVA tetramer-positive cells in IELs (*E*) and LPLs (*F*) of the stomach, small intestine, or large intestine after oral administration of OVA plus CT. C57BL/6 mice were orally administered OVA or OVA plus CT once weekly for 2 wk. IELs and LPLs were collected from mice 3 days after the second oral administration. Cells were stained with PE-labeled H-2K^b/OVA tetramer and FITC-labeled anti-mouse CD8β. Each value represents the percentage of cells expressing both indicated markers. The results are representative of three independent experiments.

α-IEL chain)-positive cells in the collected samples were examined by flow cytometry. CD103 is highly expressed on >90% of IELs (29, 30) but on only 15% of SCs (31). In the present study, CD103-positive cells occupied >90% of IELs and ~15% of SCs (data not shown). Although a small number of OVA-specific TCR-expressing cells were detected in both IELs (4.5–5.0%) and SCs (1.0–1.5%) after oral administration of OVA plus CT in comparison with control H-2K^b/PB1-positive cells, H-2K^b/OVA tetramer-positive cells were not observed in mice treated with OVA alone (Fig. 1*A*). Such OVA peptide-specific TCR-expressing cells were TCRγδ negative (data not shown) and both CD8α and β positive (Fig. 1*B*). The number of tetramer-positive cells, to which the magnitude of direct OVA-specific cytotoxicity closely corresponded, was maximal at day 7 after oral immunization with both IELs and SCs (Fig. 1*B*), but it did not correspond to NK cell activity as measured against YAC-1 targets (Fig. 1*C*). The results clearly demonstrate that direct OVA-specific CTL cytotoxicity is dominantly observed in mucosal IELs after primary oral administration of OVA plus CT.

Augmentation and kinetics of direct OVA-specific cytotoxicity by CD8αβ CTLs among IELs and SCs via oral boosting with OVA plus CT at day 7 after the primary administration

As shown above, because only 4.5–5.0% of IELs were temporarily activated by a one-shot oral administration, we extensively examined the effect of oral boosting with OVA plus CT at various days after primary immunization. The number of H-2K^b/OVA tetramer-positive cells was significantly enhanced among IELs but not among SCs when primed mice were boosted (Fig. 2*A*). Such an effect was highest when mice were boosted at day 7 after initial

priming (data not shown). Tetramer-positive cells were again
AQ: K TCRβ-, CD8α-, and CD8β-positive IELs and their number peaked at day 3 after boosting (Fig. 2*B*). Correspondingly, direct OVA-specific cytotoxicity was greatly enhanced among IELs and the maximal cytotoxicity of IELs was observed at day 3 after boosting (Fig. 2*C*), although such direct cytotoxicity appeared to be completely lost in SCs (Fig. 2*C*). Nonetheless, SCs showed good epitope-specific cytotoxicity similar to that of IELs when they were restimulated in vitro with irradiated E.G7-OVA (Fig. 2*D*), suggesting that the priming effect by the oral administration of OVA plus CT also remained in systemic SCs.

It should be noted that the memory of OVA-specific CTLs persisted among IELs but not SCs. When secondary boosting with OVA plus CT was performed even 6 mo after primary boosting at day 7, the number of H-2K^b/OVA tetramer-positive cells was still detected at ~6% in IELs, and they showed remarkable direct cytotoxicity of ~84.5% against E.G7-OVA cells and 58.4% against EL4 cells pulsed with OVA peptide 3 days after secondary boosting (data not shown). Again, we could not detect any measurable direct cytotoxicity in the SCs of secondary boosted mice (data not shown).

Both CTA and CTB subunits are required to induce direct OVA-specific cytotoxicity in IELs

CT is comprised of a single A subunit, CTA, and five B subunits, CTB. When OVA was administered orally to mice with either 10 μg of CTA or an equal amount of CTB, H-2K^b/OVA-tetramer-positive cells as well as direct OVA-specific cytotoxicity could not
F3 be detected in IELs (Fig. 3, *A* and *B*) and SCs (data not shown), although a significant number of tetramer-positive cells and strong direct OVA-specific cytotoxicity were observed among IELs of mice administered orally with OVA plus 10 μg of intact CT (Fig. 3, *A* and *B*). Even when using 50 μg of CTA or CTB for the administration of OVA, direct cytotoxicity was not observed (data not shown); therefore, both CTA and CTB subunits are required to induce direct Ag-specific cytotoxicity.

Effects of oral administration and booting with OVA plus CT on OVA-expressing tumor growth established in the stomach

We then examined in vivo antitumor effects of oral administration with tumor Ag plus CT on already established tumors growing in mice. C57BL/6 mice were implanted with 5 × 10^6 syngeneic
F4 E.G7-OVA cells into the muscle layer of the stomach (Fig. 4*A*). Three days later, tumor-bearing mice (Fig. 4*A*) were orally administered various combinations of OVA plus adjuvant and boosted with the same materials 7 days after the initial oral administration. To our surprise, tumor growth in the stomach of mice orally administered OVA plus CT twice was visually (Fig. 4*B*) and significantly ($p < 0.05$; Fig. 4*C*) suppressed on day 18 after tumor implantation as compared with other control groups such as OVA plus CTB or CT alone. However, when tumor-bearing mice were orally administered OVA plus CT once and without boosting, no statistically significant suppression was observed on day 18 as compared with untreated control mice, although a slight suppressive effect could be seen (Fig. 4*D*). Therefore, two oral administrations of tumor-Ag plus CT with an appropriate interval induced significant ongoing tumor suppression.

As previously shown, direct OVA-specific cytotoxicity among small intestinal IELs was greatly enhanced after boosting with OVA plus CT (Fig. 2, *A*, *B*, and *C*). We also examined whether direct OVA-specific CTLs were induced in the IELs and LPLs of the stomach, small intestine, and large intestine from boosted mice in which gastric tumor growth was significantly suppressed. We observed an increase in the number of H-2K^b/OVA tetramer-positive

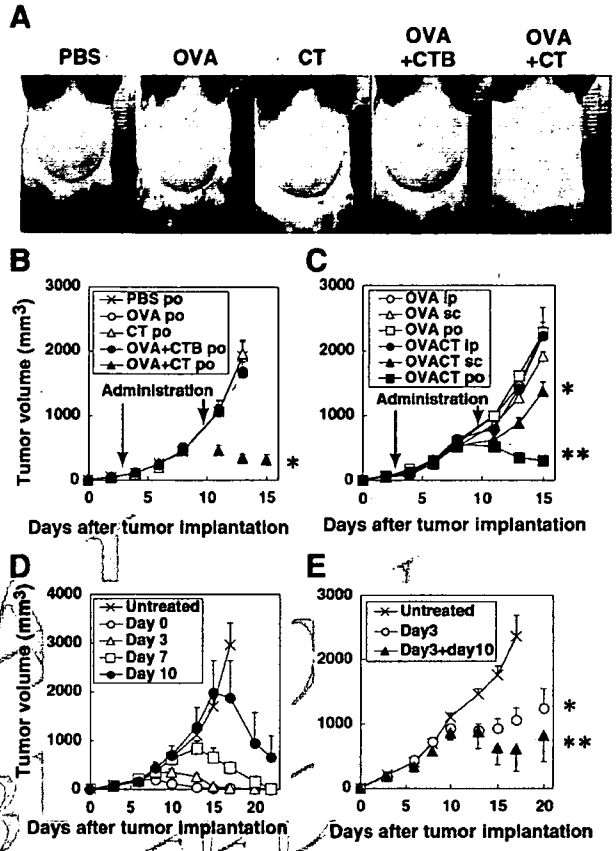

FIGURE 5. Suppression of intradermal tumor growth by oral administration with OVA plus CT. C57BL/6 mice were implanted intradermally with 5 × 10^6 E.G7-OVA cells. Three days later, tumor-bearing mice were orally administered PBS, OVA, CT, OVA plus CTB subunit, or OVA plus CT. Seven days later, the second oral administration was performed in the same manner. *A*, Visual suppressive effect of oral inoculation of OVA plus CT on dermal tumor growth. *B*, Tumor volumes were calculated based on the formula described in *Materials and Methods* and the results are shown as the mean ± SEM. Results were obtained from 5–6 mice per group. The asterisk (*) indicates statistically significant difference between the OVA plus CT group (closed triangle) and any other group at 11 days ($p < 0.05$) and 13 days ($p < 0.005$) after tumor inoculation. *C*, C57BL/6 mice were implanted intradermally with E.G7-OVA cells. Three days later, tumor-bearing mice were intraperitoneally (ip), subcutaneously (sc), or orally (po) administered OVA alone or OVA plus CT. Seven days later, the second treatment was performed in the same manner. The results are shown as the mean of tumor volumes ± SEM. Results were obtained from 5–6 mice per group. The asterisk (*) shows statistically significant differences ($p < 0.05$) between the s.c. OVA plus CT group (▲) and the s.c. OVA alone group at days 11, 13, and 15 after tumor implantation, and the two asterisks (**) indicate significant differences ($p < 0.01$) between the oral OVA plus CT group (■) and the oral OVA alone group on the same days. *D*, C57BL/6 mice were implanted intradermally with E.G7-OVA cells. The mice were orally administered once with OVA plus CT at day 0, 3, 7, or 10 after tumor implantation. The results are shown as the mean of tumor volumes ± SEM. Results were obtained from 10–12 mice per group. In single orally administered groups, significant tumor regression ($p < 0.05$) was observed at 7 days after oral administration compared with the untreated group. *E*, C57BL/6 mice were implanted intradermally with E.G7-OVA cells. Three days later, tumor-bearing mice were orally administered a low dose (10 mg) of OVA plus CT. Seven days later, some orally administered mice were boosted in the same manner. The results obtained from 5- mice per group are shown as the mean of tumor volumes ± SEM. The asterisk (*) indicates statistically significant differences ($p < 0.01$) between the nonboosted (○) and untreated mice (×) groups at days 15 and 17 after tumor implantation, and the two asterisks (**) indicate significant differences ($p < 0.005$) between the boosted (▲) and untreated groups on the same days.

balt6/zim-jimm/zim-jimm/zim00608/zim6741-08z | xppws | S=1 | 1/24/08 | 12:54 | 4/Color Figure(s): F4-6 | Art: 6741 | Input-ALK/MP

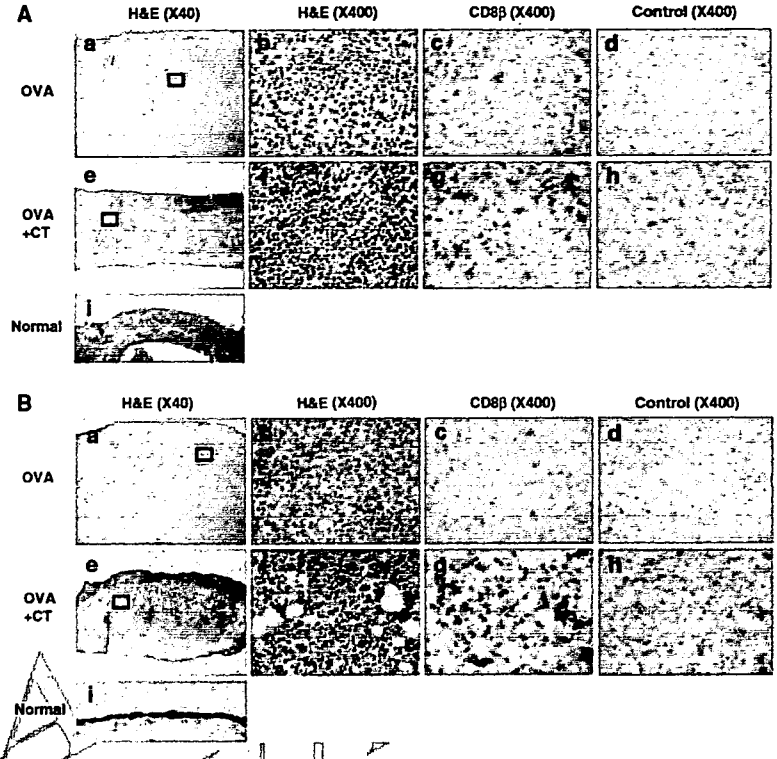

FIGURE 6. Infiltration of CD8$\alpha\beta$ positive lymphocytes into tumor tissues in mice orally administered OVA plus CT. C57BL/6 mice were implanted with 5×10^6 E.G7-OVA cells into the muscle layer of the stomach (*A*, *a–h*) or skin (*B*, *a–h*). Three days later, tumor-bearing mice were orally administered OVA (*A*, *a–d*, and *B*, *a–d*) or OVA plus CT (*A*, *e–h* and *B*, *e–h*). Seven days later, the second oral administration was performed in the same manner. Gastric and dermal tumor tissues were removed from mice 3 days after the second oral boost. Frozen sections of tumor tissues and normal tissues were prepared and stained with H&E (*A*, *a*, *b*, *e*, *f*, and *i* and *B*, *a*, *b*, *e*, *f*, and *i*) or immunohistochemically stained with biotin-conjugated rat anti-CD8β mAb (*A*, *c* and *g*, and *B*, *c* and *g*) or control isotype-matched rat IgG2a Ab (*A*, *d* and *h*, and *B*, *d* and *h*). Image magnification is either ×40 (*A*, *a*, *e*, and *i* and *B*, *a*, *e*, and *i*) or ×400 (*A*, *b–d* and *f–h* and *B*, *b–d* and *f–h*). *A*, *b* and *f* and *B*, *b* and *f* are enlarged images (×400) of the squared areas in the images (×40) of *A*, *a* and *e* and *B*, *a* and *e*, respectively.

cells among IELs in the stomach (38.4%) as well as the small (18.9%) and large intestine (4.9%) of tumor-suppressed mice (Fig. 4*E*) and also among LPLs in the stomach (21.1%) as well as the small (1.0%) and large (0.6%) intestine (Fig. 4*F*). Thus, the ability of LPLs to suppress tumor growth may be weaker than that of IELs. The results suggest that oral administration of Ag plus intact CT with appropriate mucosal boosting apparently suppressed the already established tumor growth in gastric tissue, particularly after oral boosting, probably through the activation of Ag-specific CTLs in the mucosal compartment.

Effects of oral administration and boosting with OVA plus CT on already established OVA-expressing dermal tumor growth

Next, we investigated the effect of the oral administration of tumor Ag plus CT on tumor growth in the skin, where the digestive tract is not directly associated. Mice were implanted with 5×10^6 E.G7-OVA cells intradermally. Three days later, tumor-bearing mice were orally administered various combinations of OVA plus adjuvant and boosted with the same materials 7 days after the initial oral administration. Interestingly, intradermal tumor growth was again strongly suppressed visually 11 days after tumor implantation in the dermis of mice orally administered OVA plus CT as compared with various other groups (Fig. 5*A*). This visual effect was confirmed by calculating the volume of the tumors established at day 11 and day 13 in each group ($p < 0.05$ and $p < 0.005$, respectively; Fig. 5*B*). We also examined the effect of the administration of tumor Ag plus CT via various routes on intradermal tumor growth. Although a slight suppression was observed by s.c. inoculation of OVA plus CT, tumor growth was not suppressed at all by i.p. administration in comparison with the oral treatment group (Fig. 5*C*). It should be noted that tumor growth in the dermis was markedly suppressed even by a single oral administration of OVA plus CT on day 0, 3, 7, or 10 after tumor implantation (Fig. 5*D*). In each group, tumor growth was suppressed ($p < 0.05$) and the tumor volume was small around 7 days after oral administration. Unexpectedly, there was almost no difference in the suppressive effects on tumor growth between mice treated with a single administration and boosted mice showing much stronger direct cytotoxicity (data not shown). However, when the dosage quantity of OVA was decreased by one-tenth, tumor growth in boosted mice was more significantly ($p < 0.005$) suppressed than in nonboosted mice ($p < 0.01$; Fig. 5*E*). Collectively, the results indicate that the oral administration of tumor Ag plus CT with appropriate mucosal boosting may induce a remarkable suppression of already established tumor growth in the skin via mucosally generated CTLs.

Infiltration of CD8$\alpha\beta$-positive cells in suppressed tumor tissues

We thus examined whether OVA-specific CD8$\alpha\beta$-positive CTLs were actually seen in suppressed tumor tissues such as the stomach and dermis. To determine tumor-infiltrating CD8$\alpha\beta^+$ cells, immunohistochemical staining was performed using biotin-conjugated rat anti-CD8β Ab (Fig. 6*A*, *c* and *g* and *B*, *c* and *g*) or control isotype-matched rat IgG2a Ab (Fig. 6*A*, *d* and *h* and *B*, *d* and *h*). Indeed, although mononuclear cells were seen in the gastric tumor tissues of mice treated with OVA alone, CD8$\alpha\beta$-positive cells were not observed at all (Fig. 6*A*, *a–d*). In contrast, infiltration of inflammatory mononuclear cells together with CD8$\alpha\beta$-positive cells was observed in suppressed gastric tumor tissues (Fig. 6*Ag*). As shown in Fig. 6*Ai*, normal gastric tissue is composed of the epithelium, lamina propria, lamina muscularis mucosae, muscle layer, and serosa from the inside surface in sequence. As compared with normal gastric tissue, a great number of large tumor cells (EG.7-OVA) were mainly found between the lamina muscularis mucosae and serosa of tumor-implanted tissues (Fig. 6*A*, *a* and *b*) and the infiltration of tumor cells into the lamina propria over the lamina muscularis mucosae was also observed (data not shown). However, in suppressed gastric tumor tissues (Fig. 6*Ae*) the tumor cell layer under the lamina muscularis mucosae was markedly thinner than that of an unsuppressed tumor (Fig. 6*Aa*), in which

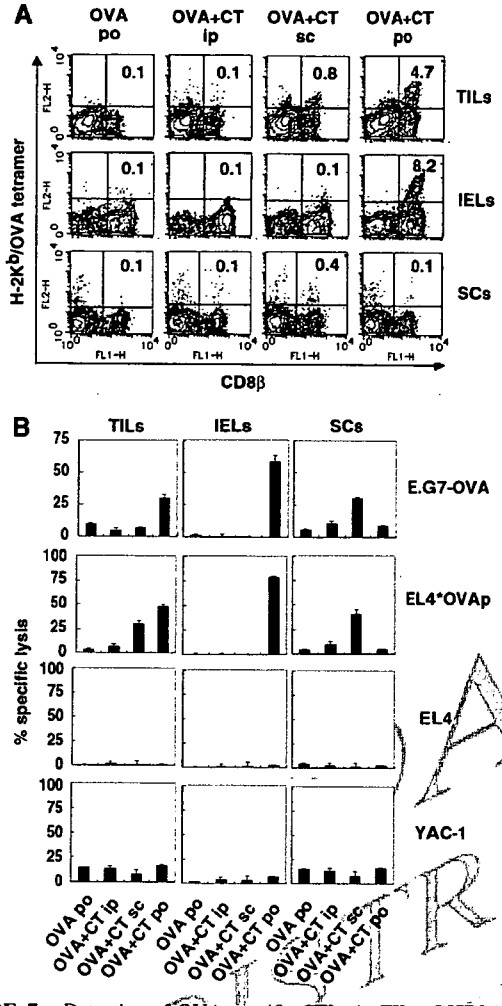

FIGURE 7. Detection of OVA-specific CTLs in TILs. C57BL/6 mice were implanted intradermally with E.G7-OVA cells. Three days later, mice were orally (po), subcutaneously (sc), or intraperitoneally (ip) administered OVA plus CT or orally treated with OVA. Seven days later, the second oral administration was performed in the same manner. TILs, IELs, and SCs were collected from mice 3 days after the second oral administration. *A*, TILs, IELs and SCs were double-stained with PE-labeled H-2K^b/OVA tetramer and FITC-labeled anti-mouse CD8β. *B*, OVA-specific CTL responses of TILs, IELs, and SCs were measured by a ^{51}Cr-release assay using E.G7-OVA cells, YAC-1 cells, and EL4 cells pulsed with or without OVA peptide as targets. The E:T ratio is 5:1 in TILs, or 100:1 in IELs and SCs. The results are shown as the mean ± SD in triplicate of pooled cells from three mice. The results are representative of three independent experiments.

tumor cells almost never infiltrated the lamina propria over the lamina muscularis mucosae. Similarly, as for dermal tumor tissues, mononuclear cells together with CD8$\alpha\beta$-positive cells were not observed in mice treated with OVA alone (Fig. 6*B*, *a–d*), whereas the infiltration of a large number of mononuclear cells and CD8$\alpha\beta$-positive cells was observed in suppressed dermal tumor tissues (Fig. 6*B*, *e–g*). Dermal tumor sections were not stained with control isotype-matched rat IgG (Fig. 6*B*, *d* and *h*). As shown in Fig. 6*Bi*, normal skin is composed of epidermides and dermis from the surface in sequence. In tumor cell-implanted dermal tissues, although the infiltration of mononuclear cells or CD8$\alpha\beta$-positive cells was not observed, many large tumor cells were found thickly beneath the epidermides (Fig. 6*B*, *a* and *b*); however, when tumor cell-implanted mice were treated with OVA plus CT, most tumor cells became necrotic or apoptotic (Fig. 6*B*, *e* and *f*).

Measurement of tumor-specific cytotoxic activity by tumor-infiltrating cells in tumor-suppressed mice

To confirm whether infiltrated CD8$\alpha\beta$-positive T cells achieved OVA-specific cytotoxicity, we isolated TILs containing both mononuclear cells and CD8$\alpha\beta$-positive T cells from suppressed dermal tumor tissues as well as from their IELs and SCs. As expected, the number of H-2K^b/OVA tetramer-positive cells increased in both the TILs and IELs but not in the SCs of mice bearing suppressed tumors induced by oral administration with OVA plus CT as compared with mice inoculated with OVA plus CT via another route (Fig. 7*A*), and those increased tetramer-positive cells showed significant direct OVA-specific CTL activity (Fig. 7*B*). It should be noted that, although the number of increased cells specific for the H-2K^b/OVA tetramer was small in mice inoculated with OVA plus CT s.c., both the TILs (0.8%) and the SCs (0.4%) but not the IELs (0.1%) of the mice represented a detectable level of direct OVA-specific cytotoxicity (Fig. 7*B*). These findings suggest that s.c. immunization with Ag plus CT may preferably activate systemic (splenic) Ag-specific CTLs rather than local (intraepithelial) CTLs. Moreover, NK cell cytotoxicity determined against YAC-1 cells was not observed in TILs, IELs, and SCs by oral, s.c., or i.p. immunization of OVA plus CT (Fig. 7*B*), indicating that the suppression of tumor growth was mainly mediated by CD8$\alpha\beta$ CTLs rather than by NK cell cytotoxicity.

F7

AQ: M

Discussion

In the present study we demonstrated that when OVA plus intact CT was orally administered into mice, direct OVA-specific cytotoxicity was dominantly induced in IELs rather than SCs after the first oral priming, and direct OVA-specific cytotoxicity was remarkably expanded in IELs but not in SCs after oral boosting with the same doses of OVA plus CT. Such OVA-specific CTLs were thymic conventional K^b class I MHC molecule-restricted TCR$\alpha\beta^+$ CD8$\alpha\beta$ T cells (32). Moreover, the growth of the OVA-expressing tumor E.G7-OVA thymoma, established previously either in the stomach or dermis, was significantly suppressed by the oral administration of OVA plus CT. Furthermore, marked infiltration of OVA-specific TCR$\alpha\beta^+$ CD8$\alpha\beta$ CTLs with direct cytotoxicity in reduced tumor tissues was observed. These results suggest that activated CTLs with specific cytotoxicity generated at mucosal compartments by oral administration with OVA plus intact CT may be responsible for already established tumor regression.

The majority of tumor regression studies associated with activation of the immune system have focused on systemic immunity observed in the spleen, lymph nodes, and circulating blood rather than local mucosal immunity seen in gut IELs. Those studies have demonstrated only preventative results for tumor establishment by preadministration of tumor Ag plus a suitable adjuvant. In addition, to our knowledge only one study has been shown to suppress already established tumor growth by activating and expanding tumor infiltrating CD8$^+$ CTLs (23). In that study, i.v. vaccination with DCs prepulsed ex vivo with OVA-CT at day 3 and boosted at day 10 after OVA-expressing E.G7 tumor injection induced complete rejection of a visible tumor within 3 wk after the first treatment. Although the inoculation route and the materials for vaccination were different from ours, the timing of the priming and boosting to induce the suppression of already established tumor growth correlated exactly, suggesting that their methods may also initiate strong mucosal direct cytotoxicity mediated through CD8$^+$ CTLs.

Similar to our findings, they also showed that immunization with OVA-CT but not with CTB-conjugated OVA (OVA-CTB)-prepulsed DCs could successfully induce complete rejection of already established tumor growth, although OVA-CTB-prepulsed DC inoculation prevented tumor establishment but not ongoing tumor growth in the skin. Moreover, they insisted that OVA has to be coupled to CT and should be loaded onto DCs for therapeutic DC vaccination based on the observation that neither OVA-CT nor DCs pulsed with unconjugated OVA plus CT could prevent tumor progression. Nonetheless, our findings shown here apparently indicate that we were able to induce effective suppression of ongoing tumor growth by simple oral administration with unconjugated OVA and CT. These results suggest that we may control already established tumor growth at the surface compartments by activating mucosal $CD8^+$ CTLs via orally administered tumor Ag with a suitable mucosal adjuvant. Also, when OVA-CT is orally administered, the conjugation between OVA and CT may be broken through digestion by enzymes secreted in the gastrointestinal tract. Recently, we have reported that modification of OVA in the gastrointestinal tract is essential for oral tolerance induction against OVA (33). Therefore, it is possible that gastrointestinal digestion or modification of OVA may facilitate the delivery of OVA Ag into DCs, critical APCs for OVA-specific CTL induction.

For the efficient induction of such OVA-specific CTLs in vivo using DCs, Eriksson et al. have reported that OVA-CT-prepulsed DC immunization required at least two DC injections, reflecting the priming/boosting procedure (23); however, we have observed that a single oral administration of OVA plus CT seems sufficient to induce effective CTLs to prevent E.G7-OVA thymoma growth, particularly in the skin. This may be because mucosally activated CTLs through oral immunization may be more potent than systemically activated CTLs to suppress transplanted tumors at the mucosal compartment, and oral administration of OVA plus CT seems more efficient to induce mucosal CTLs than i.v. Ag-loaded DC inoculation. Further studies will be needed to explain the differences.

Although both CT-conjugated-OVA and CTB-conjugated OVA are cross-presented by MHC class I in DCs, only CT-OVA but not CTB-OVA cross-primes OVA-specific $CD8^+$ CTLs in vivo (23, 34). Additionally, DCs pulsed with intact OVA alone cannot cross-present and cross-prime CTLs (23). For the cross-priming of Ag-specific CTLs by Ag-captured immature DCs, maturation signaling via some surface molecules such as TLR-3 in those DCs is essential (35, 36). Although whole CT up-regulates the expression of MHC class II, B7.1, and B7.2 molecules on DCs in vitro, neither CTA nor CTB alone up-regulates the levels of surface markers on DCs (37, 38). Also, the binding of CTB to GM1 on DCs seems necessary to efficiently take up both CT itself and Ag and to induce cross-presentation by MHC class I molecules on DCs, whereas CTA may not be taken up to affect DCs. When DCs from GM1-lacking mice were matured in vitro, CT failed to up-regulate the expression of maturation markers and, thus, the binding of B subunits in CT to GM1 molecules on DCs is essential for the induction of DC maturation (37). It has been reported that CTA is required to not only assist in maturation but also to generate the migration of DCs (39, 40); therefore, CTB-mediated matured DCs can initiate their migration to secondary lymphoid organs and colocalization with naive T cells (38). Indeed, CT-loaded but not CTB-loaded DCs could migrate from marginal zones to T cell zones in the spleen (39) and from the subepithelial dome region to T cell zones in PPs (40); therefore, both CTA and CTB were essential for cross-priming CTLs in vivo and neither CTA nor CTB alone could induce CTLs at various compartments (Fig. 3). Taken together, although the detailed mechanisms of efficient Ag presentation via MHC class I and the maturation and migration of DCs by CT are still unknown, digested OVA might be efficiently captured by immature gut mucosal DCs in the presence of CTB and the captured Ag may be cross-presented by MHC class I during DC maturation and migration in the presence of CTA, resulting in the induction of mucosal class I MHC molecule-restricted CTLs that may cause the regression of previously established tumors.

OVA-specific $CD8^+$ CTLs were induced among not only the IELs but also the LPLs of the stomach, small intestine, and large intestine by oral administration of OVA plus CT, a higher percentage of OVA-specific CD8 CTLs was observed in the stomach, small intestine, and large intestine in order, and more specific CTLs were always detected among IELs than among LPLs (Fig. 4, *E* and *F*). Thus, CTLs are much easier to be induced in the upper and more superficial portions of the gastrointestinal tract when Ags are orally administrated with intact CT.

It has been reported that DCs in gastric mucosa are increased in *Helicobacter pylori* (*Hp*)-infected mice and that the response of DCs and T cells to *Hp* Ag is critical for *Hp*-induced gastritis (41). In the present study, Ag-specific CTLs in the stomach might be generated by mucosally activated DCs in the presence of CT and infiltrate-implanted gastric tumor tissues. It is possible that intestinally activated CTLs might migrate to the tumor-implanted stomach, which might also cause CTL infiltration. Actually, such effector CTLs usually express high levels of $\alpha_4\beta_7$ integrin and can home in to the gastric (42), and small and large intestinal mucosa (43) where mucosal addressin cell-adhesion molecule-1 (MadCAM-1), the ligand of $\alpha_4\beta_7$ integrin, is constitutively expressed by post-capillary endothelial cells in small (44, 45) and large intestinal lamina propria (46). Moreover, the number of gastric $\alpha_4\beta_7^{high}$ T cells increased markedly by oral administration of CT in mice (42). It has also been reported that MAdCAM-1 expression is increased in the gastric mucosa after oral administration with cholera vaccine composed of CTB and formalin-inactivated *V. cholerae* (47); therefore, MadCAM-1-expression in gastric mucosa and the recruitment of effector $\alpha4\beta7^{high}$ T cells to gastric mucosa might be enhanced by oral administration of the CT adjuvant and, thus, OVA-specific effector CTLs might efficiently infiltrate the OVA Ag-expressing tumor region in the stomach.

In the present study, we found that the growth of dermally implanted tumors was also suppressed by the oral administration of tumor Ag plus whole intact CT. The actual mechanisms for such suppression remains to be elucidated, but there are at least three distinct possibilities: first, the migration of Ag-specific CTLs from the gastrointestinal tract to the skin; second, the migration of Ag-presenting DCs activated in the mucosal compartments by CT; and third, the migration of both cells from the gastrointestinal tract to the skin at the same time. It has been reported that the levels of CCR4 expression, which is associated with T cell homing to the skin, are increased in gastric T cells by infection with *Hp* in humans (48). Moreover, mucosal DCs that take up Ag might migrate to regional lymph nodes near the dermal tumor and prime the CTLs there, and the CTLs could effectively infiltrate dermal tumor tissue. Indeed, Belyakov et al. demonstrated an opposite mechanism in which skin-derived DCs containing heat-labile enterotoxin of *Escherichia coli* migrated to PPs and induced mucosal CTLs by transcutaneous immunization of an Ag and CT (49). Although the detailed mechanisms of this migration of DCs between skin and mucosa are unknown, they have clearly shown that DCs can migrate between the mucosa and skin. We are currently comparing the alteration of DCs in the mucosal compartment, spleen, and lymph nodes after oral administration of an Ag plus natural CT.

Unfortunately, such natural CT is not an appropriate mucosal adjuvant for human clinical investigation (50); however, studies

using natural CT would provide important and critical information about the effect of CT that would be useful for mucosal immune activation. Based on the findings obtained by using natural CT in a mouse model system, we could establish much safer protocols with a mutant CT (51) that induces adenosine diphosphate ribosylation and cyclic adenosine monophosphate formation, which may prevent severe diarrhea as well as retain adjuvant properties. Taken together, an artificial CT-based vaccine targeting DCs may provide a strategy for efficient CTL induction and avirulent mucosal cancer vaccination.

Our data also indicate that E.G7-OVA tumor growth was suppressed by OVA-specific CTLs but not NK cells (Fig. 7*B*). Vaccination with OVA-CT-pulsed DC protects against E.G7-OVA tumor development in vivo in wild-type, NK-depleted, and CD4-deficient mice but not in CD8-deficient mice (34), indicating that the E.G7-OVA tumor might be controlled by CD8 T cells but not by NK cells or CD4 T cells. In fact, TILs in the suppressed tumor did not show any NK-related cytotoxicity (Fig. 7*B*). Moreover, it has been demonstrated that in vitro pretreatment of NK cells with CT inhibits NK cell killing of tumor (YAC-1 or P815), because G proteins in NK cell membranes are ADP ribosylated with CT and ribosylation inhibits the lysis of tumor cells (52); therefore, NK cells do not seem to be involved in the suppression of E.G7-OVA growth in vivo.

It has been shown that activated CTLs but not naive CTLs can represent antitumor (22) or antivirus (12) responses in vivo. In the present study, already established E.G7 tumor growth can be suppressed only when OVA-specific CTLs that show specific cytotoxicity without requiring in vitro restimulation are induced, particularly in the mucosal compartment. To our knowledge, this is the first demonstration of the visual suppression of already established tumor growth by the simple oral administration of tumor Ag plus mucosal adjuvant. The findings shown in the present study herald a new era for cancer immunotherapy.

Acknowledgments

We thank Dr. Yoshihiro Kumagai and Yoshihiko Norose for useful discussions and advice.

Disclosures

The authors have no financial conflict of interest.

References

1. Franks, L. M., and M. A. Knowles. 2005. What is cancer? In *Introduction to the Cellular and Molecular Biology of Cancer*, 4th Ed. M. A. Knowles and P. J. Selby, eds. Oxford University Press, New York, pp. 1–24.
2. Finn, O. J. 2003. Cancer vaccines: between the idea and the reality. *Nat. Rev. Immunol.* 3: 630–641.
3. Czerkinsky, C., F. Anjuere, J. R. McGhee, A. George-Chandy, J. Holmgren, M. P. Kieny, K. Fujiyashi, J. F. Mestecky, V. Pierrefite-Carle, C. Rask, and J. B. Sun. 1999. Mucosal immunity and tolerance: relevance to vaccine development. *Immunol. Rev.* 170: 197–222.
4. Yuki, Y., and H. Kiyono. 2003. New generation of mucosal adjuvants for the induction of protective immunity. *Rev. Med. Virol.* 13: 293–310.
5. Takahashi, H. 2003. Antigen presentation in vaccine development. *Comp. Immunol. Microbiol. Infect. Dis.* 26: 309–328.
6. Hayday, A., E. Theodoridis, E. Ramsburg, and J. Shires. 2001. Intraepithelial lymphocytes: exploring the third way in immunology. *Nat. Immunol.* 2: 997–1003.
7. Offit, P. A., and K. I. Dudzik. 1989. Rotavirus-specific cytotoxic T lymphocytes appear at the intestinal mucosal surface after rotavirus infection. *J. Virol.* 63: 3507–3512.
8. Chardes, T., D. Buzoni-Gatel, A. Lepage, F. Bernard, and D. Bout. 1994. *Toxoplasma gondii* oral infection induces specific cytotoxic CD8 $\alpha\beta^+$ Thy-1$^+$ gut intraepithelial lymphocytes, lytic for parasite-infected enterocytes. *J. Immunol.* 153: 4596–4603.
9. Muller, S., M. Buhler-Jungo, and C. Mueller. 2000. Intestinal intraepithelial lymphocytes exert potent protective cytotoxic activity during an acute virus infection. *J. Immunol.* 164: 1986–1994.
10. Taunk, J., A. I. Roberts, and E. C. Ebert. 1992. Spontaneous cytotoxicity of human intraepithelial lymphocytes against epithelial cell tumors. *Gastroenterology* 102: 69–75.
11. Roberts, A. I., S. M. O'Connell, L. Biancone, R. E. Brolin, and E. C. Ebert. 1993. Spontaneous cytotoxicity of intestinal intraepithelial lymphocytes: clues to the mechanism. *Clin. Exp. Immunol.* 94: 527–532.
12. Kuribayashi, H., A. Wakabayashi, M. Shimizu, H. Kaneko, Y. Norose, Y. Nakagawa, J. Wang, Y. Kumagai, D. H. Margulies, and H. Takahashi. 2004. Resistance to viral infection by intraepithelial lymphocytes in HIV-1 P18-I10-specific T-cell receptor transgenic mice. *Biochem. Biophys. Res. Commun.* 316: 356–363.
13. Takahashi, H., J. Cohen, A. Hosmalin, K. B. Cease, R. Houghten, J. L. Cornette, C. DeLisi, B. Moss, R. N. Germain, and J. A. Berzofsky. 1988. An immunodominant epitope of the human immunodeficiency virus envelope glycoprotein gp160 recognized by class I major histocompatibility complex molecule-restricted murine cytotoxic T lymphocytes. *Proc. Natl. Acad. Sci. USA* 85: 3105–3109.
14. Williams, N. A., T. R. Hirst, and T. O. Nashar. 1999. Immune modulation by the cholera-like enterotoxins: from adjuvant to therapeutic. *Immunol. Today* 20: 95–101.
15. Lencer, W. I., and B. Tsai. 2003. The intracellular voyage of cholera toxin: going retro. *Trends Biochem. Sci.* 28: 639–645.
16. Elson, C. O., and W. Ealding. 1984. Generalized systemic and mucosal immunity in mice after mucosal stimulation with cholera toxin. *J. Immunol.* 132: 2736–2741.
17. Marinaro, M., H. F. Staats, T. Hiroi, R. J. Jackson, M. Coste, P. N. Boyaka, N. Okahashi, M. Yamamoto, H. Kiyono, H. Bluethmann, et al. 1995. Mucosal adjuvant effect of cholera toxin in mice results from induction of T helper 2 (Th2) cells and IL-4. *J. Immunol.* 155: 4621–4629.
18. Bowen, J. C., S. K. Nair, R. Reddy, and B. T. Rouse. 1994. Cholera toxin acts as a potent adjuvant for the induction of cytotoxic T-lymphocyte responses with non-replicating antigens. *Immunology* 81: 338–342.
19. Carbone, F. R., and M. J. Bevan. 1989. Induction of ovalbumin-specific cytotoxic T cells by in vivo peptide immunization. *J. Exp. Med.* 169: 603–612.
20. Moore, M. W., F. R. Carbone, and M. J. Bevan. 1988. Introduction of soluble protein into the class I pathway of antigen processing and presentation. *Cell* 54: 777–785.
21. Porgador, A., H. F. Staats, S. Faiola, E. Gilboa, and T. J. Palker. 1997. Intranasal immunization with CTL epitope peptides from HIV-1 or ovalbumin and the mucosal adjuvant cholera toxin induces peptide-specific CTLs and protection against tumor development in vivo. *J. Immunol.* 158: 834–841.
22. Dalyot-Herman, N., O. F. Bathe, and T. R. Malek. 2000. Reversal of CD8$^+$ T cell ignorance and induction of anti-tumor immunity by peptide-pulsed APC. *J. Immunol.* 165: 6731–6737.
23. Eriksson, K., J. B. Sun, I. Nordstrom, M. Fredriksson, M. Lindblad, B. L. Li, and J. Holmgren. 2004. Coupling of antigen to cholera toxin for dendritic cell vaccination promotes the induction of MHC class I-restricted cytotoxic T cells and the rejection of a cognate antigen-expressing model tumor. *Eur. J. Immunol.* 34: 1272–1281.
24. Taguchi, T., J. R. McGhee, R. L. Coffman, K. W. Beagley, J. H. Eldridge, K. Takatsu, and H. Kiyono. 1990. Analysis of Th1 and Th2 cells in murine gut-associated tissues: frequencies of CD4$^+$ and CD8$^+$ T cells that secrete IFN-γ and IL-5. *J. Immunol.* 145: 68–77.
25. Takahashi, M., E. Osono, Y. Nakagawa, J. Wang, J. A. Berzofsky, D. H. Margulies, and H. Takahashi. 2002. Rapid induction of apoptosis in CD8$^+$ HIV-1 envelope-specific murine CTLs by short exposure to antigenic peptide. *J. Immunol.* 169: 6588–6593.
26. Semple, J. W., and M. R. Szewczuk. 1986. Natural killer cells in murine muscular dystrophy: IV. Characterization of Percoll fractionated splenic and thymic natural killer cells and natural killer-sensitive thymocyte targets. *Clin. Immunol. Immunopathol.* 41: 116–129.
27. Belz, G. T., W. Xie, and P. C. Doherty. 2001. Diversity of epitope and cytokine profiles for primary and secondary influenza a virus-specific CD8$^+$ T cell responses. *J. Immunol.* 166: 4627–4633.
28. Nakatsuka, K., H. Sugiyama, Y. Nakagawa, and H. Takahashi. 1999. Purification of antigenic peptide from murine hepatoma cells recognized by class-I major histocompatibility complex molecule-restricted cytotoxic T-lymphocytes induced with B7-1-gene-transfected hepatoma cells. *J. Hepatol.* 30: 1119–1129.
29. Kilshaw, P. J., and K. C. Baker. 1988. A unique surface antigen on intraepithelial lymphocytes in the mouse. *Immunol. Lett.* 18: 149–154.
30. Russell, G. J., C. M. Parker, K. L. Cepek, D. A. Mandelbrot, A. Sood, E. Mizoguchi, E. C. Ebert, M. B. Brenner, and A. K. Bhan. 1994. Distinct structural and functional epitopes of the α E β 7 integrin. *Eur. J. Immunol.* 24: 2832–2841.
31. Lefrancois, L., T. A. Barrett, W. L. Havran, and L. Puddington. 1994. Developmental expression of the α IEL β 7 integrin on T cell receptor γ δ and T cell receptor α β T cells. *Eur. J. Immunol.* 24: 635–640.
32. Rocha, B., P. Vassalli, and D. Guy-Grand. 1994. Thymic and extrathymic origins of gut intraepithelial lymphocyte populations in mice. *J. Exp. Med.* 180: 681–686.
33. Wakabayashi, A., Y. Kumagai, E. Watari, M. Shimizu, M. Utsuyama, K. Hirokawa, and H. Takahashi. 2006. Importance of gastrointestinal ingestion and macromolecular antigens in the vein for oral tolerance induction. *Immunology* 119: 167–177.
34. Sun, J. B., K. Eriksson, B. L. Li, M. Lindblad, J. Azem, and J. Holmgren. 2004. Vaccination with dendritic cells pulsed in vitro with tumor antigen conjugated to cholera toxin efficiently induces specific tumoricidal CD8$^+$ cytotoxic lymphocytes dependent on cyclic AMP activation of dendritic cells. *Clin. Immunol.* 112: 35–44.

35. Fujimoto, C., Y. Nakagawa, K. Ohara, and H. Takahashi. 2004. Polyriboinosinic polyribocytidylic acid [poly(I:C)]/TLR3 signaling allows class I processing of exogenous protein and induction of HIV-specific $CD8^+$ cytotoxic T lymphocytes. *Int. Immunol.* 16: 55–63.
36. Schulz, O., S. S. Diebold, M. Chen, T. I. Naslund, M. A. Nolte, L. Alexopoulou, Y. T. Azuma, R. A. Flavell, P. Liljestrom, and C. Reis e Sousa. 2005. Toll-like receptor 3 promotes cross-priming to virus-infected cells. *Nature* 433: 887–892.
37. Kawamura, Y. I., R. Kawashima, Y. Shirai, R. Kato, T. Hamabata, M. Yamamoto, K. Furukawa, K. Fujihashi, J. R. McGhee, H. Hayashi, and T. Dohi. 2003. Cholera toxin activates dendritic cells through dependence on GM1-ganglioside which is mediated by NF-κB translocation. *Eur. J. Immunol.* 33: 3205–3212.
38. Gagliardi, M. C., F. Sallusto, M. Marinaro, A. Langenkamp, A. Lanzavecchia, and M. T. De Magistris. 2000. Cholera toxin induces maturation of human dendritic cells and licences them for Th2 priming. *Eur. J. Immunol.* 30: 2394–2403.
39. Grdic, D., L. Ekman, K. Schon, K. Lindgren, J. Mattsson, K. E. Magnusson, P. Ricciardi-Castagnoli, and N. Lycke. 2005. Splenic marginal zone dendritic cells mediate the cholera toxin adjuvant effect: dependence on the ADP-ribosyltransferase activity of the holotoxin. *J. Immunol.* 175: 5192–5202.
40. Shreedhar, V. K., B. L. Kelsall, and M. R. Neutra. 2003. Cholera toxin induces migration of dendritic cells from the subepithelial dome region to T- and B-cell areas of Peyer's patches. *Infect. Immun.* 71: 504–509.
41. Drakes, M. L., S. J. Czinn, and T. G. Blanchard. 2006. Regulation of murine dendritic cell immune responses by *Helicobacter felis* antigen. *Infect. Immun.* 74: 4624–4633.
42. Michetti, M., C. P. Kelly, J. P. Kraehenbuhl, H. Bouzourene, and P. Michetti. 2000. Gastric mucosal $\alpha_4\beta_7$-integrin-positive CD4 T lymphocytes and immune protection against *Helicobacter* infection in mice. *Gastroenterology* 119: 109–118.
43. Lefrancois, L., C. M. Parker, S. Olson, W. Muller, N. Wagner, M. P. Schon, and L. Puddington. 1999. The role of β_7 integrins in CD8 T cell trafficking during an antiviral immune response. *J. Exp. Med.* 189: 1631–1638.
44. Berlin, C., R. F. Bargatze, J. J. Campbell, U. H. von Andrian, M. C. Szabo, S. R. Hasslen, R. D. Nelson, E. L. Berg, S. L. Erlandsen, and E. C. Butcher. 1995. α_4 integrins mediate lymphocyte attachment and rolling under physiologic flow. *Cell* 80: 413–422.
45. Berlin, C., E. L. Berg, M. J. Briskin, D. P. Andrew, P. J. Kilshaw, B. Holzmann, I. L. Weissman, A. Hamann, and E. C. Butcher. 1993. $\alpha_4\beta_7$ integrin mediates lymphocyte binding to the mucosal vascular addressin MAdCAM-1. *Cell* 74: 185–195.
46. Streeter, P. R., E. L. Berg, B. T. Rouse, R. F. Bargatze, and E. C. Butcher. 1988. A tissue-specific endothelial cell molecule involved in lymphocyte homing. *Nature* 331: 41–46.
47. Lindholm, C., A. Naylor, E. L. Johansson, and M. Quiding-Jarbrink. 2004. Mucosal vaccination increases endothelial expression of mucosal addressin cell adhesion molecule 1 in the human gastrointestinal tract. *Infect. Immun.* 72: 1004–1009.
48. Lundgren, A., C. Trollmo, A. Edebo, A. M. Svennerholm, and B. S. Lundin. 2005. *Helicobacter pylori*-specific $CD4^+$ T cells home to and accumulate in the human *Helicobacter pylori*-infected gastric mucosa. *Infect. Immun.* 73: 5612–5619.
49. Belyakov, I. M., S. A. Hammond, J. D. Ahlers, G. M. Glenn, and J. A. Berzofsky. 2004. Transcutaneous immunization induces mucosal CTLs and protective immunity by migration of primed skin dendritic cells. *J. Clin. Invest.* 113: 998–1007.
50. Clarke, L. L., B. R. Grubb, S. E. Gabriel, O. Smithies, B. H. Koller, and R. C. Boucher. 1992. Defective epithelial chloride transport in a gene-targeted mouse model of cystic fibrosis. *Science* 257: 1125–1128.
51. Yamamoto, S., Y. Takeda, M. Yamamoto, H. Kurazono, K. Imaoka, M. Yamamoto, K. Fujihashi, M. Noda, H. Kiyono, and J. R. McGhee. 1997. Mutants in the ADP-ribosyltransferase cleft of cholera toxin lack diarrheagenicity but retain adjuvanticity. *J. Exp. Med.* 185: 1203–1210.
52. Maghazachi, A. A., A. Al-Aoukaty, C. Naper, K. M. Torgersen, and B. Rolstad. 1996. Preferential involvement of Go and Gz proteins in mediating rat natural killer cell lysis of allogeneic and tumor target cells. *J. Immunol.* 157: 5308–5314.

Available online at www.sciencedirect.com
ScienceDirect
Antiviral Research 75 (2007) 152–158
Antiviral Research
www.elsevier.com/locate/antiviral

Suppression of virus replication via down-modulation of mitochondrial short chain enoyl-CoA hydratase in human glioblastoma cells

Megumi Takahashi [a], Eiji Watari [a], Eiji Shinya [a], Takako Shimizu [b], Hidemi Takahashi [a,*]

[a] *Department of Microbiology and Immunology, Nippon Medical School, 1-1-5 Sendagi, Bunkyo-ku, Tokyo 113-8602, Japan*
[b] *Department of Environmental Medicine, Nippon Medical School, 1-1-5 Sendagi, Bunkyo-ku, Tokyo 113-8602, Japan*

Received 17 August 2006; received in revised form 17 February 2007; accepted 21 February 2007

Abstract

Several viruses have been demonstrated to be the etiologic agent in chronic progressive diseases, associated with persistence; however, major questions concerning the pathogenic mechanisms of viral persistence are still unanswered. With the aim of identifying host cellular proteins that may play a role in viral replication, we established long-term persistently infected human glioblastoma cell lines with mutant measles virus (MV) and analyzed the host proteins by two-dimensional gel electrophoresis (2-DE) with mass spectrometry. We observed significant down-modulation in the expression of mitochondrial short chain enoyl-CoA hydratase (ECHS), which catalyzes the β-oxidation pathway of fatty acid. Knockdown of this gene by a short interference RNA (siRNA) apparently impaired wild-type MV replication and the cytopathic effects (CPEs) of MV were significantly reduced in siRNA-transfected cells. These findings will shed light upon a new important notion for the interaction between virus replication and lipid metabolism in host cells and might provide a new strategy for virus control.

Keywords: Measles virus; Persistent infection; Mitochondrial short chain enoyl-CoA hydratase; β-Oxidation; Short interference RNA

1. Introduction

A persistent viral infection is one in which a virus in a replicating or non-replicating form persists in the host beyond the normal recovery and elimination period for that particular viral infection. Although the dynamics of immune responses after acute viral infection are well studied and very consistent, the patterns of responses noted during persistent infection are more complex and differ depending on the infection. Two essential ingredients have been identified in the current understanding of persistent virus infection. The first is an immune response that is ineffectual in recognizing and clearing a virus and/or virus-infected cells; the second is that viruses can regulate the expression of both their own genes and host genes to achieve residence in a non-lytic state within the cells they infect. However, knowledge of how viral genes and cellular factors interact to cause persistence is incomplete in most instances.

In our laboratory, we have established several monkey kidney cell lines persistently infected with temperature-sensitive mutants of measles virus (MV) (Watari et al., 1979, 2001). Many aspects of these cells such as interferon production have been investigated but fail to provide a coherent mechanistic explanation for viral persistence. In this study we established a human glioblastoma cell line persistently infected with mutant measles virus, because MV persistently infect and replicate in human cells of neuronal origin and elicit subacute sclerosing panencephalitis (SSPE) in humans (Horta-Barbosa et al., 1969; Payne et al., 1969). We analyzed these persistently infected cells using two-dimensional gel electrophoresis (2-DE) in combination with tandem mass spectrometry (MS/MS), which allows us to study the alterations of host proteins during virus adaptation to the cells.

Here, we found that the expression level of mitochondrial short chain enoyl-CoA hydratase (ECHS), which catalyzes the β-oxidation pathway of fatty acid, was specifically down-modulated in persistently infected cells. Moreover, knockdown of the gene by short interference RNA (siRNA) apparently impaired wild-type MV replication, and cytopathic effects (CPEs) by MV infection were significantly reduced in siRNA-transfected cells. If one of the hallmarks of persistent infection is stable and low-level virus replication, our findings suggest that some host cellular proteins associated with lipid metabolism

* Corresponding author. Tel.: +81 3 3822 2131x5381; fax: +81 3 3316 1904.
E-mail address: htkuhkai@nms.ac.jp (H. Takahashi).

0166-3542/$ – see front matter © 2007 Elsevier B.V. All rights reserved.
doi:10.1016/j.antiviral.2007.02.002

might contribute to the regulation of virus replication followed by the establishment of persistent infection.

2. Materials and methods

2.1. Cell culture and viruses

Human glioblastoma cells, A172 and U373MG (Bender et al., 1992), were gifts from Dr. Hiroshi Takahashi (Department of Neurosurgery, Nippon Medical School, Tokyo, Japan) and were grown in Eagle's minimum essential medium (MEM, Nikken BioMedical Laboratory, Tokyo, Japan) supplemented with 10% heat-inactivated fetal calf serum, 100 U/ml of penicillin and 100 μg/ml of streptomycin. As described recently (Watari et al., 2005), wild-type Edmonston strain measles virus (Rapp clone 5) was grown and titrated on Vero cells. A temperature-sensitive mutant virus P-448 was established from Rapp clone 5 described previously (Yamaji et al., 1975). To establish persistently infected cells, A172 cells grown as monolayers were infected with P-448 mutant virus at a multiplicity of 0.1. Infected cells were passaged for the first time at 24 days' post-infection. Since the first passage, cells have been passaged weekly and were termed 448-A172 cells. For virus titration, serial tenfold dilutions of cell supernatants and cell lysates were inoculated into each of four wells of Vero cells and then incubated for 5 days. After incubation, wells were scored for CPE and we determined the dilution as $TCID_{50}$/ml at which 50% of the wells were infected.

2.2. Cell staining

For morphological analysis, cells grown on the culture plate were washed with PBS and fixed in 4% paraformaldehyde or acetone for 10 min, then cells were stained with hematoxylin solution. For immunochemical analysis, a cytospin preparation of A172 cells infected with wild-type MV and 448-A172 cells was incubated with vaccinated human serum with MV. After washing, they were overlaid with fluorescein isothiocyanate-conjugated goat anti-human antibody (Tago, Inc., Burlingame, CA).

2.3. Preparation of protein samples

The cell pellet (5×10^6 cells/sample) was disrupted in sample re-hydration buffer (8 M urea, 2% CHAPS, 0.5% ZOOM Carrier Ampholytes, 20 mM dithiothreitol (DTT), 0.002% bromophenol blue; Invitrogen, Carlsbad, CA) at room temperature for 15 min. The lysate was separated by centrifugation at $10{,}000 \times g$ for 5 min to yield supernatant that was stored at −80 °C until use. To visualize low-abundance proteins more efficiently, we prepared sub-cellular fraction of cells using a proteome extraction kit (Calbiochem, Darmstadt, Germany).

2.4. Two-dimensional gel electrophoresis

Cell lysate in re-hydration buffer was applied to ZOOM strips (pH 4–7, Invitrogen) in a total volume of 155 μl. After re-hydration for 16 h at room temperature, proteins were separated by isoelectrofocusing (IEF) at room temperature and 50 mA/strip with the following linear voltage increases: 200 V for 20 min, 450 V for 15 min, 750 V for 15 min, and 2000 V for 30 min. The strips were equilibrated in 50 mM Tris containing 6 M urea, 30% glycerol, 2% sodium dodecylsulfate (SDS) and 2% DTT for 20 min. The second dimension was performed on 13% SDS-polyacrylamide gels. Separated protein spots were fixed and stained on the gel with a silver staining kit (Nacalai Tesque, Kyoto, Japan). Differential spots were excised from silver-stained gels and treated with 20 μg of trypsin/ml in 50 mM ammonium bicarbonate buffer at 37 °C overnight. After in-gel digestion, the digested solution was transferred into a clean tube and dried under vacuum. The resulting samples were dissolved in 20 μl of 2% acetonitrile and 0.1% trifluoroacetic acid, and applied to LC–MS/MS analysis.

2.5. Identification of protein spots

Analysis was performed using an LC–MS/MS system with RP-mLC composed of a Paradigm MS4 dual solvent delivery system (Michrom BioResources, Auburn, CA), a HTC PAL auto sampler with two 10-port injector valves (CTC Analytics), Finnigan LCQ Deca XP plus (Thermo Electron, Waltham, MA) equipped with NSI sources (AMR Inc., Tokyo, Japan). The mass spectrometer was operated in data-dependent acquisition mode in which MS acquisition with a mass range of m/z 450–2000 was automatically switched to MS/MS acquisition under the automated control of Xcalibur software. The capillary exit of the electrospray ion source was set at 70 V, the octapole at 3 V, and the capillary temperature at 250 °C. A counter flow of helium was used as nebulizing gas. Each sample was injected onto a capillary RP column, MAGIC C18 (3 mm, 200 Å, 50 m × 0.2 m i.d., Michrom BioResources) with an acetonitrile linear gradient of 3 ml/min in formic acid 0.1%, from 2 to 60%. The HPLC column was rinsed with 90% acetonitrile in 0.1% formic acid between each injection.

2.6. siRNA transfection

A172 cells were plated in 48-well tissue culture plates at 1×10^5 cells/well in 150 μl MEM on the day of transfection. Cells were transfected with 1 μl HiPerFect Transfection Reagent (Qiagen, Düsseldorf, Germany) and 1 μl siRNAs (5 nM) in a total volume of 100 μl DMEM (Sigma–Aldrich, St. Louis, MO) according to the manufacturer's protocol. At 48 h after transfection, cells were infected with viruses and their growth on transfected cells was analyzed using the $TCID_{50}$ protocol. The siRNA oligonucleotides targeted the ECHS gene at position 864–884 (termed #864: aaagagaaaggccaacttcaa), 865–885 (termed #865: aagagaaaggccaacttcaaa), 1088–1108 (termed #1088: ctggqgcqccttctaaatcta), and 1245–1265 (termed #1245: cagatgctgattaaagtgata). These siRNAs were synthesized by Qiagen. Non-silencing siRNA with no known homology to mammalian genes was a commercially available duplex (Qiagen) and was used as control siRNA.

2.7. Quantitative RT-PCR

RNA was prepared from siRNA-transfected A172 cells using RNAeasy (Qiagen). One microgram of RNA was incubated for 1 h at 42 °C after adding 20 U of RNase inhibitors (TaKaRa, Bio Inc., Otsu, Japan), 0.2 mM deoxynucleoside triphosphates, 2.5 nM random primers, 11 U of Rous associated virus 2 reverse transcriptase (TaKaRa) and reverse transcriptase buffer to a final volume of 20 μl. One microlitre of RT reaction mixture was used as a template for real-time PCR using SYBR Green PCR Master Mix (Applied Biosystems, Foster City, CA) with the following primers specific for ECHS (forward, cgctgctgtcaatggctatg, and reverse, cttggcgtcctgggctgaga), β-actin (forward, tcacccacactgcccatctacga, and reverse, cagcggaaccgctcattgccaatgg), MV-NP protein (forward, tcagtagagcggttggaccc, and reverse, ggcccggtttctctgtagct), MV-H protein (forward, ttcatcgggcagccatctac, and reverse, ctctgaggtgtcctcaggcc), MV-F protein (forward, gcgagcctggaaactactaatca, and reverse, ccctgaacagccaatatcatctc). The amount of each ECHS mRNA was normalized to that of β-actin mRNA in the same sample.

2.8. Measurement of cell growth

Single cell suspensions were seeded at a density of 5×10^4 cells/well on 96-well microtiter plates. After 1–3 days of incubation, the cells were pulse-labeled with 0.5 μCi methyl-^{3}H-thymidine/well for the last 8 h, and were then harvested and counted using a β-counter (1450 Microbeta Trilux; Wallac, Gaithersburg, MD).

2.9. Western blotting

A172 cells treated with or without siRNA were infected with MV. After 2 days' infection, cells were lysed in 30 μl of lysis buffer (1% Nonidet P-40, 140 mM NaCl, 20 mM Tris–HCl (pH 8.0), 2 mM EDTA, 1 mM sodium orthovanadate, 1 mM PMSF, and 50 mM monoiodoacetamide) on ice for 15 min. After centrifugation at 20,400 × *g* for 15 min, proteins in cell lysates were separated by 10% SDS-PAGE under reducing conditions and transferred to a nylon membrane. The blots were probed with vaccinated human serum with MV or mouse anti-β-actin (clone AC-74, Sigma, St. Louis, MO) followed by peroxidase-

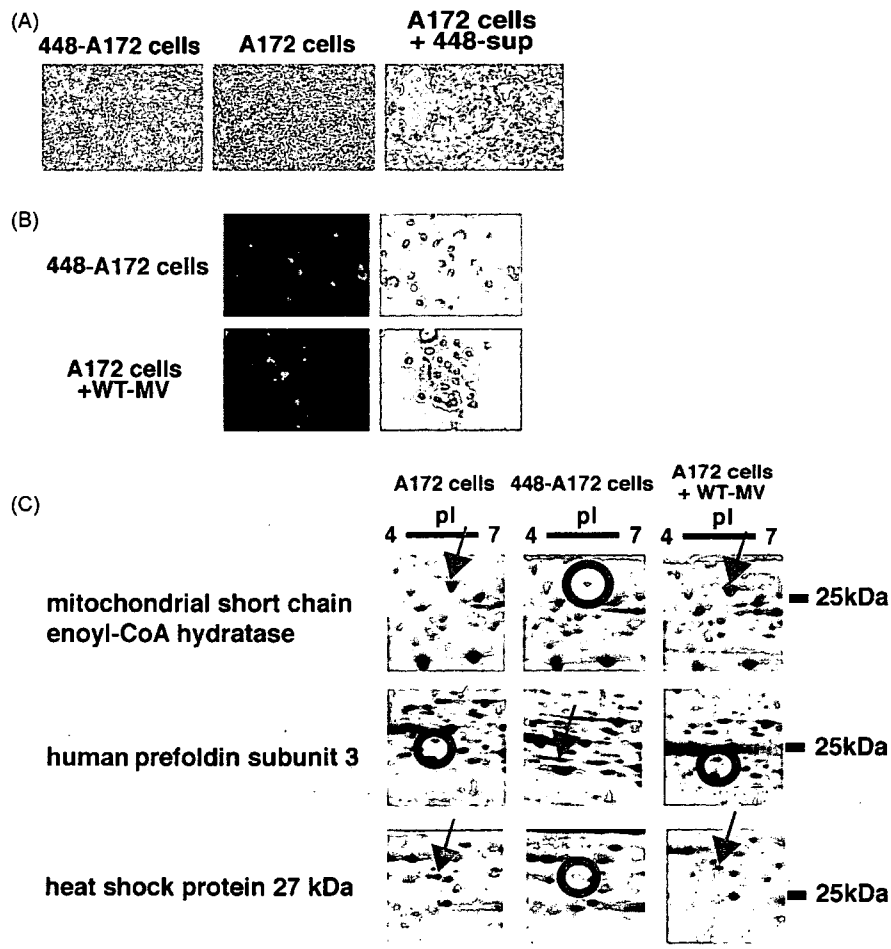

Fig. 1. Characterization of 448-A172 cells persistently infected mutant MV. (A) Morphology of 448-A172 cells (left), A172 cells (middle), and A172 cells treated with supernatants from 448-A172 cells. Cells were stained with hematoxylin solution. (B) Detection of virus antigens with vaccinated human serum with MV in 448-A172 cells (upper) or A172 cells infected with wild-type MV (lower). (C) Silver-stained two-dimensional gels of A172 cells (left column), 448-A172 cells (middle column), or A172 cells infected with wild-type MV (right column). Mitochondrial short-chain enoyl-CoA hydratase (ECHS) was detected in whole cell fraction, human prefoldin subunit 3 was detected in cytosolic fraction, and heat shock protein 27 kDa was detected in nucleus fraction.

conjugated rabbit anti-human IgG (MP Biomedicals, Irvine, CA) or goat anti-mouse IgG (Jackson ImmunoResearch, West Grove, PA). Bands were visualized using a tetramethylbenzidine substrate kit (Vector, Burlingame, CA).

3. Results

3.1. Establishment and analysis of a cell line persistently infected with temperature-sensitive mutant measles virus

To investigate the mechanisms underlying virus persistence, we established a human glioblastoma cell line persistently infected with a temperature-sensitive mutant MV named 448-A172 after about 50 days of infection. The appearance of the 448-A172 cell line was indistinguishable from intact uninfected A172 cells (Fig. 1A). Thus, the situation of persistent MV infection in 448-A172 cells was examined by the detection of intracellular viral antigens using an immunofluorescent technique. As shown in Fig. 1B, viral antigens were mainly observed in the cytoplasms of 448-A172 cells, and infectious virions from cells could be obtained and titrated on Vero cell monolayers. Indeed, culture supernatants harvested on day 4 contained measurable amounts of viruses (10^4 $TCID_{50}$/ml) that induced syncytial cell formation for intact A172 cells (Fig. 1A).

3.2. Identification of proteins crucial for persistent infection in the established 448-A172 cell line

These findings suggest that such persistent infection did not depend on the type of virion but rather on host cellular conditions; therefore, to explore the possible mechanisms involved in persistent infection, we precisely compared the cellular proteins between 448-A172 cells and A172 cells infected with or without wild-type MV using 2-DE with p*I* values in the range of 4–7 to obtain a greater resolution in protein separation. The 2-DE image of cellular proteins after silver staining is shown in Fig. 1C. For the assessment of differentially expressed proteins, protein spots clearly altered in 448-A172 cells were considered. We did find three altered proteins, which were then characterized by mass spectrometry and identified as mitochondrial short chain enoyl-CoA hydratase, human prefoldin subunit 3, and heat shock protein 27 kDa.

3.3. Inhibition of ECHS expression with specific siRNA

Among those three proteins, we focused on investigating the functional role of ECHS for viral replication, because ECHS protein is more abundant than other proteins in intact A172 cells and the amount of ECHS is obviously reduced in 448-A172 cells. Using quantitative RT-PCR analysis quantifying ECHS transcripts relative to that of β-actin from 448-A172 cells, we confirmed that the expression levels of ECHS mRNA in 448-A172 cells was decreased to less than 10% in comparison with intact A172 cells (data not shown). Then, ECHS-specific siRNAs were prepared to evaluate the potential involvement of ECHS in regulating the replication of MV. Four different siRNAs were used to specifically knockdown the expression of ECHS in intact

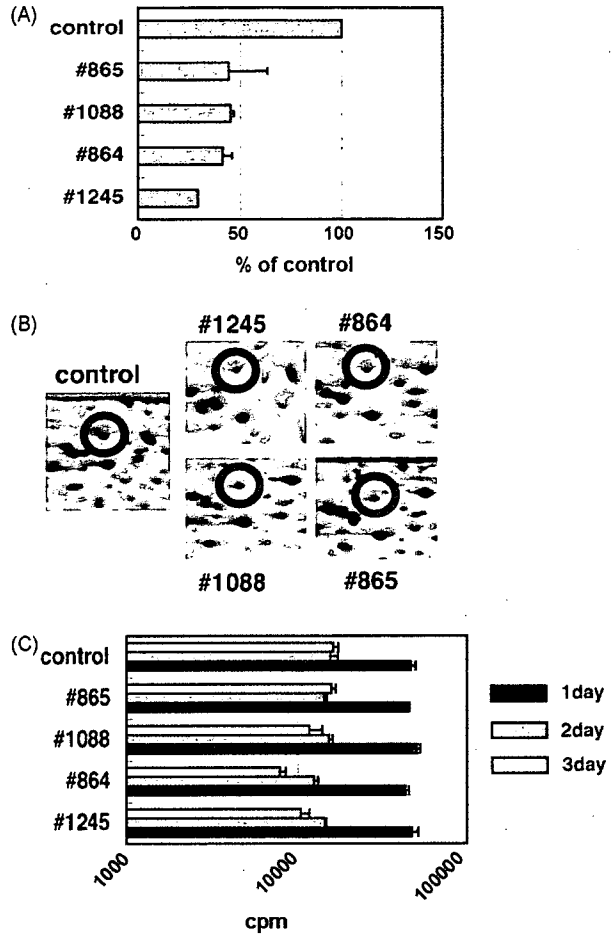

Fig. 2. Effect of siRNA transfection on A172 cells. (A) A172 cells were transfected with each siRNA. Total RNA was isolated from cells 24 h after transfection and was subjected to quantitative RT-PCR specific for ECHS or β-actin primer. Data were normalized to the amount of β-actin mRNA and are expressed as percentages of the normalized value for control siRNA-transfected cells. Values are the mean ± standard deviation (S.D.) of at least three experiments. (B) A172 cells were transfected with each siRNA. After 48 h incubation, cells were lysed and subjected to 2-DE analysis. Gels were visualized with silver staining. (C) A172 cells were transfected with each siRNA. After 1–3 days' incubation, the cells were pulse-labeled with 0.5 μCi/well methyl-^{3}H-thymidine for the last 8 h.

A172 cells. Twenty-four or 48 h post-transfection with a siRNA, mRNA and protein levels of ECHS in A172 cells were reduced up to 30–45% of control siRNA-transfected cells (Fig. 2A and B). As ECHS catalyzes the second step in the β-oxidation pathway of fatty acid metabolism, down-modulation of ECHS might result in the deficient production of energy-yielding substrates via β-oxidation. Therefore, we examined the effect of ECHS suppression on cell proliferation using the ^{3}H-thymidine uptake method. Although siRNA had little effect on cell proliferation until 2 days after transfection, the reduction of ^{3}H-thymidine uptake was observed in three siRNA-transfected cells, but no dead cells were detected 3 days after transfection (Fig. 2C).

3.4. Inhibition of MV replication by ECHS siRNA in A172 cells

To see whether the treatment of cells with ECHS-specific siRNA can inhibit MV replication, we examined their inhibitory

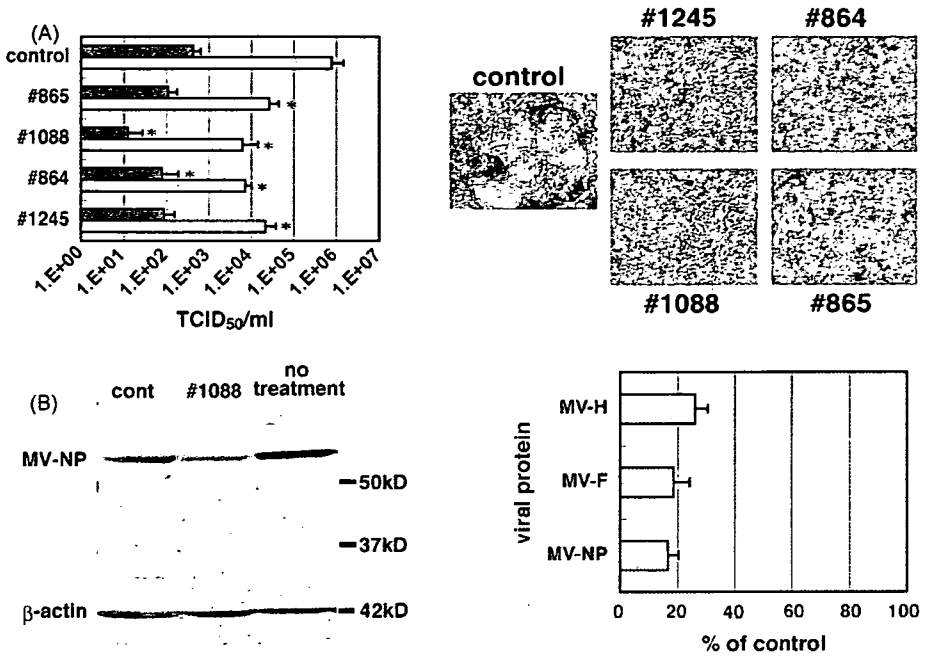

Fig. 3. Effect of siRNA transfection on MV replication. (A) A172 cells were transfected with each siRNA. After 48 h incubation, A172 cells were infected with wild-type MV, and then both cells (gray bars) and supernatants (charcoal bars) were harvested at 48 h after infection followed by determination of the virus titer (left). Data are expressed as the virus titer ($TCID_{50}$) and are the means ± S.D. of values of at least three independent experiments. $^{*}P < 0.05$ vs. the value of cells transfected with control siRNA (Student's *t*-test). Cells were stained with hematoxylin solution after 48 h infection (right). (B, left) A172 cells treated with or without siRNA were infected with MV. After 2 days' infection, cells were lysed in 30 μl of lysis buffer, and proteins in lysates were separated in 10% polyacrylaminde gel and blotted on a nylon membrane. The blot was probed with vaccinated human serum with MV (upper column) or mouse anti-β-actin antibody (lower column). (B, right) A172 cells treated with or without siRNA were infected with MV. After 2 days' infection, total RNA was isolated from cells 24 h after transfection and subjected to quantitative RT-PCR specific for MV-NP protein, MV-F protein or MV-H protein primer. Data were normalized to the amount of β-actin mRNA and are expressed as percentages of the normalized value for control siRNA-transfected cells. Values are the mean ± S.D. of at least three experiments.

effect on intact A172 cells. Forty-eight hours post-transfection with siRNA, A172 cells were infected with wild-type MV at a multiplicity of infection (moi) of 0.1. At 48 h after infection, culture supernatants and cells were harvested, serially diluted, and the virus titer determined (expressed as $TCID_{50}$/ml). As shown in Fig. 3A, we observed the efficient inhibition of MV replication after transfection with four distinct siRNAs. Indeed, when #1088 siRNA was used, inhibition was so pronounced that culture supernatants contained only a few viruses. CPE by MV infection observed at 48 h post-infection in control and ECHS siRNA-transfected groups is also shown in Fig. 3A. There is an apparent marked reduction of CPE in all siRNA-transfected cells. This was confirmed by titrating the virions yielded between control and siRNA-transfected cells. Moreover, Western blot analysis showed that transfection of A172 cells with #1088 siRNA reduced the accumulation of viral protein compared to cells transfected with control siRNA or without siRNA. This protein reduction was due to a decrease in the expression of viral mRNA (Fig. 3B).

3.5. *Effect of ECHS siRNA on other virus replication*

Next, to determine if ECHS is also involved in the replication of other RNA viruses, siRNA-transfected A172 cells were infected with vesicular stomatitis virus (VSV) or semliki forest virus (SFV). As demonstrated in Fig. 4A, targeting ECHS mRNA also significantly inhibited both VSV and SFV replication in A172 cells. Similar to MV infection, CPEs were not detected in all siRNA-transfected A172 cells at 24 h after VSV or SFV infection (data not shown).

ECHS catalyzes the β-oxidation pathway of fatty acid. To further analyze the involvement of β-oxidation in virus replication, we examined the effect of etomoxir (Sigma), an inhibitor of carnitine palmitoyltransferase that inhibits mitochondrial β-oxidation, on MV replication in A172 cells. Treatment of A172 cells with etomoxir resulted in the suppression of MV replication in a dose-dependent manner (Fig. 4B). These results suggest that β-oxidation might be involved in MV replication.

We also observed that treatment of A172 cells with IFN-β (1000 IU/ml) effectively inhibited MV replication by approximately 100 times (Fig. 4B), indicating that down-modulation of ECHS potency with siRNA corresponds to treatment with a high titer of IFN-β to inhibit virus replication. Recently, it was reported that siRNA treatment could nonspecifically induce IFN-mediated innate immune responses (Sledz and Williams, 2004); however, it was unlikely that IFN mediated protection in our experiments, because a large amount of IFN-α was originally produced in intact A172 cells but IFN-β was not detected in culture supernatants from intact or siRNA-transfected A172 cells (data not shown).

To extend the results in A172 cells, we further tested the ability of siRNAs to inhibit virus replication in other glioblastoma cells, U373MG. When U373MG cells were transfected with each siRNA and then infected with MV at a moi of 0.1

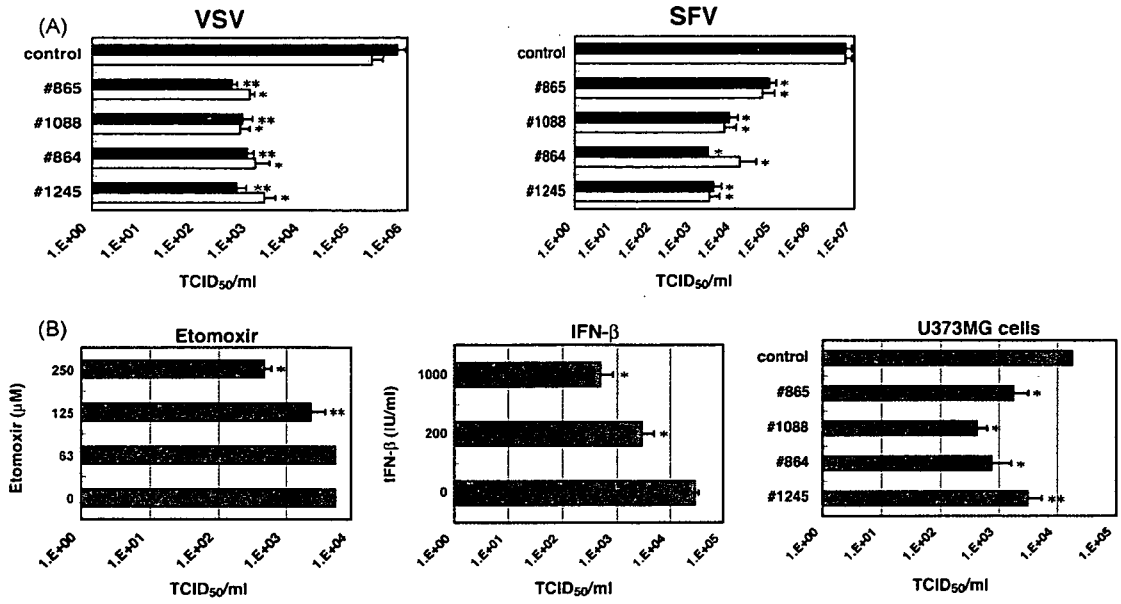

Fig. 4. Effect of siRNA transfection on other virus replication. (A) A172 cells were transfected with each siRNA. After 48 h incubation, A172 cells were infected with VSV (left) or SFV (right) at a moi of 0.1, and then cells (gray bars) and supernatants (charcoal bars) were harvested at 24 h after infection followed by determination of the virus titer. (B) A172 cells were treated with the indicated concentration of etomoxir (left). After 48 h incubation, A172 cells were infected with wild-type MV, and then supernatants were harvested at 72 h after infection followed by the assay for determination of the virus titer. A172 cells were treated with the indicated concentration of IFN-β (middle). After 24 h incubation, cells were infected with wild-type MV, and then supernatants were harvested at 48 h after infection followed by determination of the virus titer. U373MG cells were transfected with each siRNA (right). After 48 h incubation, U373MG cells were infected with wild-type MV, and then supernatants were harvested at 48 h after infection followed by determination of the virus titer. Data are expressed as the virus titer ($TCID_{50}$) and are the means ± standard deviations (S.D.) of values of at least three independent experiments. (A and B) $^{*}P < 0.02$, and $^{**}P < 0.05$ vs. the value of cells transfected with control siRNA or treated without reagents.

at 48 h post-transfection, siRNA, especially #864 and #1088, significantly inhibited virus replication (Fig. 4B). Moreover, to confirm whether stable infection with mutant MV in other cells induce the down-modulation of ECHS expression as well as 448-A172 cells, we are now attempting to establish a cell line persistently infected with mutant MV using U373MG cells.

4. Discussion

In this study, we have found that the expression of ECHS protein was significantly down-modulated in cells persistently infected with temperature-sensitive mutant MV. Moreover, similar to conventional MV, the mutant MV produced and secreted from persistently infected cells showed the capacity to induce syncytial formation upon infection to normal A172 human glioblastoma cells, indicating that such persistent infection is not due to the type of virion but rather to host cellular conditions. We thus speculate the ECHS gene as an essential host cellular gene utilized for virus replication, and conducted experiments to inhibit host cellular ECHS with siRNA by the gene-transfer technique. As expected, the replication of wild-type MV was specifically blocked by siRNA via knockdown of the ECHS gene.

ECHS catalyzes the second step in the physiologically important β-oxidation pathway of fatty acid metabolism (Agnihotri and Liu, 2003). In mammals, fatty acid oxidation occurs in mitochondria, peroxisomes, and smooth endoplasmic reticulum. Although mitochondria and peroxisomes oxidize fatty acids via β-oxidation, smooth endoplasmic reticulum metabolizes fatty acids by ω-oxidation. Such mitochondrial β-oxidation is responsible for oxidation in the major portion of short- (<C8), medium- (C8-12), and long- (C14-20) chain fatty acids and, in that process, constitutes the primary source of energy derived from fatty acids. The catalytic mechanism of ECHS has been studied in great depth through a combination of kinetic, spectroscopic, and structural techniques (Kim and Battaile, 2002); however, the expression and gene regulation of this enzyme have not been fully elucidated. Several reports have shown that the expression level of ECHS was decreased in cancer cell lines and carcinoma (Balabanov et al., 2001; Fratelli et al., 2003; Hwa et al., 2005; Sakata et al., 1998). Although the biological significance of ECHS in human cancer has not been confirmed, regulation of this enzyme by a carcinogen might have a role in the proliferation and differentiation of normal cells. On the other hand, very few reports refer to the interaction between ECHS and microbial infections. Only Yokoyama et al. have reported that the expression level of ECHS was decreased in hepatocellular carcinoma from patients infected with hepatitis C virus (Yokoyama et al., 2004).

Although we have not yet elucidated the molecular mechanism for the regulation of MV replication by ECHS, down-modulation of ECHS inevitably leads to the inhibition of β-oxidation. We also found that treatment of A172 cells with etomoxir, an inhibitor of β-oxidation, effectively suppressed virus replication. These findings suggest that β-oxidation appeared to be involved in MV replication; moreover, the fact that ECHS

siRNA also effectively interfered with VSV or SFV replication in A172 cells indicates that β-oxidation might be essential for the common replication cycles of various viruses.

Recently, there have been significant advances in identifying cellular factors that promote or inhibit viral replication. In the case of HIV-1, novel factors such as APOBEC or TRIM5α have been discovered (Sheehy et al., 2002; Stremlau et al., 2004). Both proteins show anti-viral activity; in particular, APOBEC family proteins have activity in a wide variety of viruses. Consequently, up-modulation of these proteins in host cells imparts resistance to viral replication. Taken together, there may be two concepts for suppressing virus replication in host cells: the lack of an essential factor for virus replication and the presence of an efficient mechanism for controlling replication. APOBEC proteins seem to correspond only to the latter mechanism, while ECHS might correspond to both, because the impairment of β-oxidation might result in the reduction of energy-yielding substrates (acetyl-CoA and ketone bodies), which eventually leads to a shortage of ATP, and adversely cause the accumulation of both free fatty acids and toxic acyl-CoA intermediates in cells.

Although the expression level of ECHS in 448-A172 cells seemed significantly lower than that in siRNA-transfected cells, culture supernatants from the 448-A172 cells still contained measurable amounts of viruses (10^4 $TCID_{50}$/ml) and their growth rate was almost the same as #864-siRNA-transfected cells. These data suggest that other host factors relating to viral replication besides ECHS might be stably disturbed in 448-A712 cells. Indeed, we found that human prefoldin subunit 3 and heat shock protein 27 kDa seemed to down-modulate virus replication and extend cell survival (Fig. 1C). Further investigation on another host proteins must be required to understand the precise mechanisms how viral genes and cellular factors interact to cause persistent viral infection.

One of the hallmarks of persistent infection is to create an excellent intracellular status for stable and low-level virus replication. The reduction of ECHS may contribute not only to low steady-state levels of virus replication but also to the survival of virus-infected cells. The suppression of virus replication might help to prolong the asymptomatic phase of virus infection; therefore, further precise analysis of the molecular regulation of our findings shown here might cast new light on the development of novel anti-viral drugs concerned with lipid metabolism. Indeed, Sakamoto et al. recently identified an HCV replication inhibitor which prevents the de novo synthesis of sphingolipids, a major lipid raft component (Sakamoto et al., 2005).

Acknowledgements

We thank Drs. Takahiro Isono, Noriyuki Nagahara and Masayasu Minami for experimental advice on the proteomic analysis. This work was supported in part by grants from the Ministry of Education, Science, Sport, and Culture, from the Ministry of Health and Labor and Welfare, Japan, from the Japanese Health Sciences Foundation, and from the Promotion and Mutual Aid Corporation for Private School of Japan.

Appendix A. Supplementary data

Supplementary data associated with this article can be found, in the online version, at doi:10.1016/j.antiviral.2007.02.002.

References

Agnihotri, G., Liu, H.W., 2003. Enoyl-CoA hydratase. reaction, mechanism, and inhibition. Bioorg. Med. Chem. 11, 9–20.

Balabanov, S., Zimmermann, U., Protzel, C., Scharf, C., Klebingat, K.J., Walther, R., 2001. Tumour-related enzyme alterations in the clear cell type of human renal cell carcinoma identified by two-dimensional gel electrophoresis. Eur. J. Biochem. 268, 5977–5980.

Bender, H., Takahashi, H., Adachi, K., Belser, P., Liang, S.H., Prewett, M., Schrappe, M., Sutter, A., Rodeck, U., Herlyn, D., 1992. Immunotherapy of human glioma xenografts with unlabeled, 131I-, or 125I-labeled monoclonal antibody 425 to epidermal growth factor receptor. Cancer Res. 52, 121–126.

Fratelli, M., Demol, H., Puype, M., Casagrande, S., Villa, P., Eberini, I., Vandekerckhove, J., Gianazza, E., Ghezzi, P., 2003. Identification of proteins undergoing glutathionylation in oxidatively stressed hepatocytes and hepatoma cells. Proteomics 3, 1154–1161.

Horta-Barbosa, L., Fuccillo, D.A., London, W.T., Jabbour, J.T., Zeman, W., Sever, J.L., 1969. Isolation of measles virus from brain cell cultures of two patients with subacute sclerosing panencephalitis. Proc. Soc. Exp. Biol. Med. 132, 272–277.

Hwa, J.S., Park, H.J., Jung, J.H., Kam, S.C., Park, H.C., Kim, C.W., Kang, K.R., Hyun, J.S., Chung, K.H., 2005. Identification of proteins differentially expressed in the conventional renal cell carcinoma by proteomic analysis. J. Kor. Med. Sci. 20, 450–455.

Kim, J.J., Battaile, K.P., 2002. Burning fat: the structural basis of fatty acid beta-oxidation. Curr. Opin. Struct. Biol. 12, 721–728.

Payne, F.E., Baublis, J.V., Itabashi, H.H., 1969. Isolation of measles virus from cell cultures of brain from a patient with subacute sclerosing panencephalitis. N. Engl. J. Med. 281, 585–589.

Sakamoto, H., Okamoto, K., Aoki, M., Kato, H., Katsume, A., Ohta, A., Tsukuda, T., Shimma, N., Aoki, Y., Arisawa, M., Kohara, M., Sudoh, M., 2005. Host sphingolipid biosynthesis as a target for hepatitis C virus therapy. Nat. Chem. Biol. 1, 333–337.

Sakata, M., Kurachi, H., Morishige, K., Ogura, K., Yamaguchi, M., Nishio, Y., Ikegami, H., Miyake, A., Murata, Y., 1998. Messenger RNA differential display reverse-transcriptase-polymerase-chain-reaction analysis of a progestogen-suppressive gene in a human endometrial-cancer cell line. Int. J. Cancer 78, 125–129.

Sheehy, A.M., Gaddis, N.C., Choi, J.D., Malim, M.H., 2002. Isolation of a human gene that inhibits HIV-1 infection and is suppressed by the viral Vif protein. Nature 418, 646–650.

Sledz, C.A., Williams, B.R., 2004. RNA interference and double-stranded-RNA-activated pathways. Biochem. Soc. Trans. 32, 952–956.

Stremlau, M., Owens, C.M., Perron, M.J., Kiessling, M., Autissier, P., Sodroski, J., 2004. The cytoplasmic body component TRIM5alpha restricts HIV-1 infection in Old World monkeys. Nature 427, 848–853.

Watari, E., Yamanaka, A.M., Yamaji Y, M., 1979. Establishment of persistent infection of measles virus in Vero cells with special reference to the temperature-sensitivity of parent viruses. J. Nippon Med. Sch. 46, 147–150.

Watari, E., Shimizu, M., Takahashi, H., 2005. Langerhans cells stimulated by mechanical stress are susceptible to measls virus. Intervirology 48, 145–152.

Watari, E., Shinya, E., Kurane, S., Takahashi, H., 2001. Effects of cyclosporin A on cell fusion in a monkey kidney cell line persistently infected with measles virus. Intervirology 44, 209–214.

Yamaji, Y., Honda, B.F., Todome, H., Suganuma, Y., Watari, M., Iwaguchi, E., Nagashima M, H., 1975. Characterzation of temperature-sensitive mutants of measles virus: temperature-shift experiment. Jpn. J. Med. Sci. Biol. 28, 223–229.

Yokoyama, Y., Kuramitsu, Y., Takashima, M., Iizuka, N., Toda, T., Terai, S., Sakaida, I., Oka, M., Nakamura, K., Okita, K., 2004. Proteomic profiling of proteins decreased in hepatocellular carcinoma from patients infected with hepatitis C virus. Proteomics 4, 2111–2116.

Molecular Analysis of TCR and Peptide/MHC Interaction Using P18-I10-Derived Peptides with a Single D-Amino Acid Substitution

Yohko Nakagawa,* Hiroto Kikuchi,† and Hidemi Takahashi*
*Department of Microbiology and Immunology and †Department of Physics, Nippon Medical School, Tokyo 113-8602, Japan

ABSTRACT For the structural analysis of T-cell receptor (TCR) and peptide/MHC interaction, a series of peptides with a single amino acid substitution by a corresponding D-amino acid, having the same weight, size, and charge, within P18-I10 (aa318–327: RGPGRAFVTI), an immunodominant epitope of HIV-1 IIIB envelope glycoprotein, restricted by the H-2D^d class I MHC molecule, has been synthesized. Using those peptides, we have observed that the replacement at positions 324F, 325V, 326T, and 327I with each corresponding D-amino acid induced marked reduction of the potency to sensitize targets for P18-I10-specific murine CD8$^+$ cytotoxic T lymphocytes (CTLs), LINE-IIIB, recognition. To analyze further the role of amino acid at position 325, the most critical site for determining epitope specificity, we have developed a CTL line [LINE-IIIB(325D)] and its offspring clones specific for the epitope I-10(325v) having a D-valine (v) at position 325. Taking advantage of two distinct sets of CD8$^+$ CTLs restricted by the same D^d, three-dimensional structural analysis on TCR and peptide/MHC complexes by molecular modeling was performed, which indicates that the critical amino acids within the TCRs for interacting with 325V or 325v appear to belong to the complementarity-determining region 1 but not to the complementarity-determining region 3 of Vβ chain.

INTRODUCTION

Immune responses to viral infection include both humoral and cell-mediated effector mechanisms. The major effector cells in cellular immunity are CD8 molcule-expressing cytotoxic T lymphocytes (CTLs) that can recognize and kill virus-infected cells. In general, endogenously synthesized antigens such as virus-derived proteins are fragmented inside of the cells and are presented on the cell in conjunction with class I major histocompatibility complex (MHC) molecules. Such processed epitope peptides associated with the class I MHC molecules can be recognized by CTLs via their specific T cell receptors (TCRs).

The TCRs expressed on the cell surface of T lymphocytes contain similar structural patterns with immunoglobulin-like domains, comprising one variable and one constant, as well as a transmembrane domain and a short cytoplasmic tail. The specificity for T-cell recognition seems to be determined by the variable domains, TCR Vα and TCR Vβ, within two heterodimeric subsets, TCRα and TCRβ. Several recent findings have indicated that the TCRα and β heterodimers are oriented to the long axis of the epitope-peptide/MHC complex (1), in which the Vα domain appears to cover the amino-terminal half of the epitope peptide, whereas Vβ is located over the carboxyl-terminal portion of the epitope (2).

Among those variable Vα and Vβ domains, three hypervariable complementarity-determining regions (CDRs), termed CDR1, CDR2, and CDR3, seem to directly interact with the peptide/MHC complex. Because the degree of variability is the greatest in the CDR3 loop generally, and it is positioned more closely over the epitope peptide than other CDR1 and CDR2 loops, the antigen specificity has been considered to be associated with the CDR3 but not with CDR1 or CDR2, which were predicted to interact principally with the MHC molecules (3,4). Indeed, according to a recent report on the murine K^b class I MHC molecule-restricted epitope octapeptide (pKB1: KVITFIDL) recognized by KB5-C20 TCR (5), TCR plasticity is primarily restricted to the CDR3 loops of the Vβ domain. Nevertheless, recent crystallographic analyses on various TCR and peptide/MHC interactions have suggested the possibility of direct contact for both CDR1 and CDR3 in the TCRα and TCRβ chains with the antigenic peptide/MHC complex (5,6). Therefore, to understand more precise molecular interactions determining T-cell specificity through TCR-mediated peptide/MHC complex recognition, we took advantage of the following known materials to accomplish the analysis.

We have established CD8$^+$, H-2D^d class I MHC molecule-restricted murine CTL line, LINE-IIIB, specific for the envelope glycoprotein 160 (gp160) composed of ~900 amino acids derived from one of the most commonly used IIIB strains of human immunodeficiency virus type-1 (HIV-1), a causative agent for acquired immunodeficiency syndrome (AIDS) (7). Then, we have identified an immunodominant epitope within the gp160 as a 15-residue peptide, P18IIIB (aa315–329: RIQRGPGRAFVTIGK), for the LINE-IIIB recognition (7) as well as the minimal active 10-residue peptide, P18-I10 (aa318–327: RGPGRAFVTI) within P18IIIB (8). Moreover, although the position of P18IIIB is located in the hypervariable portion (termed V3 domain) of the viral envelope, the site has turned out to be recognized by various isolate-specific CTLs in an isolate-specific manner (9,10), and

Submitted August 16, 2006, and accepted for publication December 13, 2006.
Address reprint requests to Hidemi Takahashi, Department of Microbiology and Immunology, Nippon Medical School, 1-1-5 Sendagi, Bunkyo-ku, Tokyo 113-8602, Japan. Tel.: 81-3-3822-2131 ext. 5381; Fax: 81-3-3316-1904; E-mail: htkuhkai@nms.ac.jp.

0006-3495/07/04/2570/13 $2.00
doi: 10.1529/biophysj.106.095208

a number of distinct class I MHC molecules did present the P18IIIB to each specific CTL (11). Furthermore, the P18IIIB in the V3-domain was found to be overlapped with the major determinant sites for neutralizing antibodies against HIV-1 in an isolate-specific manner (12–14) and also to be recognized by CD4-positive helper T lymphocytes specific for HIV-1 in a class II MHC molecule-restricted manner (8,15). In addition, human CTLs did see the P18IIIB when presented by HLA A2 and A3 (16). These findings indicate that the P18IIIB appears to be a highly attractive epitope for the development of peptide-based vaccine against AIDS, and thus, it is important to study the precise interaction between the epitope P18IIIB and their specific TCRs to study the manner of T-cell-mediated immune responses.

Using a series of peptides with an alanine (A) substitution at each position, we observed that amino acids at positions 322R and position 324F were critical for D^d binding and that position 325V within P18-I10 was essential for interacting with TCRs (17). Also, C-terminus 327I appears to be critical for D^d binding to form the D^d-binding motif (8,18). In addition, we found the HIV-MN isolate-specific CTLs also saw the corresponding minimal active site, MNT10 (aa318–327: IGPGRAFYTT) in association with the same D^d molecules, and replacement of just a single residue, 325V with 325Y, within the P18-I10 or vice versa within the MNT10 was sufficient to reciprocally interchange the specificities for these two non-cross-reactive sets of CTLs (9,10). Thus, a single side chain at position 325 can play a critical role in determining the epitope specificity within both P18-I10 and MNT10 presented by the same class I MHC molecule D^d for $CD8^+$ CTL TCR recognition mediated by the CDRs.

It has been reported that the charge of the amino acid might also affect interaction between TCRs and peptide/MHC complexes (19). Indeed, when negatively charged glutamic acid (E) at position 436 within HIV-1-envelope-derived helper T-cell epitope T1 (aa428–443; KQIINMWQEVGKAMYA) (20) was substituted with either uncharged alanine (A) or size-conservative, uncharged glutamine (Q), stimulatory capacity of the substitute peptides for T1-specific T hybridomas was significantly enhanced, although charge-conservative aspartic acid (D) substitution did not show any enhancement (21). Moreover, substitution at position 6Q in the immunodominant CTL epitope for vesicular stomatitis virus (RGYVYQGL, VSV8) presented by K^d class I MHC molecules to a negatively charged residue such as 6E or 6D induced a change at position 93S of TCR CDR3α to a positively charged residue 93R or 93K (22). Therefore, particularly to reduce the influence of charges of each amino acid as well as the size and molecular weight on TCR-mediated recognition, a series of P18-I10-derived peptides with a single amino acid substitution by D-amino acid at each corresponding site have been synthesized. Using those D-amino acid–substituted peptides, we found apparent reduction of specific cytotoxic activity in the 325V-specific LINE-IIIB cells by the replacement of 325V with D-type valine at position 325, represented as I10(325v). Then, we attempted to establish CTL lines specific for the epitope I-10(325v) by immunization with dendritic cells pulsed with the peptide, I10(325v) (23). We have successfully generated both a 325(v)-specific CTL line and clones that did not cross-react with the original P18-I10.

Taking advantage of two distinct sets of $CD8^+$ CTL clones specific for either P18-I10 bearing L-type valine or I10(325v) having D-type valine at position 325 presented by the same MHC molecules D^d, we attempted to study the three-dimensional (3D) structural analysis on TCRs and peptide/MHC complexes. Here, using molecular modeling analysis, we would like to show that the critical amino acids for interacting with P18-I10 in determining epitope specificity appear to be the peptide DMSHET within CDR1 of Vβ7, whereas those for interacting with I10(325v) appear to be TNSHNY within CDR1 of Vβ8.3.

MATERIALS AND METHODS

Mice

Female BALB/c ($H\text{-}2^d$) mice were purchased from Charles-River Japan Inc. (Tokyo, Japan). The mice were 6 to 10 weeks of age and were maintained in a specific-pathogen-free environment. All experiments were performed according to the guidelines of the NIH Guide for the Care and Use of Laboratory Animals.

Synthetic peptides

Peptides were synthesized and purified as described previously (24). Table 1 summarizes the peptides used in this study; L-amino acids are represented as capital letters, and D-amino acids as lower-case letters.

Transfectants

BALB/c.3T3 ($H\text{-}2^d$) fibroblast transfectants expressing the HIV-1 gp160 of IIIB isolate (15-12) and control transfectants with selectable marker genes (Neo) (7, 17) were used for the CTL assay. Murine L-cells ($H\text{-}2^k$) transfected with $H\text{-}2D^d$ (T4.8.3) (25), $H\text{-}2L^d$ (T.1.1.1) (25), and $H\text{-}2K^d$ (B4III2) (26) were used to determine the MHC class I restriction of the generated CTL line and clones.

Monoclonal antibodies

We used fluorescein isothiocyanate-conjugated antimouse CD3 (145-2C11), $\alpha\beta$TCR (H57-597), CD4 (RM4-5), and CD8 (53-6.7) monoclonal antibodies (PharMingen, San Diego, CA) to determine the cell surface molecules of the established CTL lines and clones.

CTL lines and clones

The P18-I10-specific CTL line, LINE-IIIB, was generated as described previously (7). Based on a previously reported procedure (23), a CTL line specific for I10(325v) was generated from spleen cells of BALB/c mice immunized with I10(325v)-pulsed splenic dendritic cells. Briefly, immune spleen cells were restimulated in vitro with mitomycin C-treated I10(325v)-pulsed syngeneic BALB/c.3T3 fibroblasts in 24-well culture plates containing 1.5 ml of complete T-cell medium composed of RPMI 1640 medium

TABLE 1 Sequences of substituted peptides used in this study

Peptide	Sequence*															
Residue No.	315										325					329
P18IIIB	R	I	Q	R	G	P	G	R	A	F	V	T	I	G	K	
P18-I10				R	G	P	G	R	A	F	V	T	I			
I10(325I)											I					
I10(325L)											L					
I10(325A)											A					
I10(325Y)											Y					
I10(325F)											F					
I10(325H)											H					
I10(325T)											T					
I10(325S)											S					
I10(325E)											E					
I10(325K)											K					
I10(325R)											R					
I10(325P)											P					
I10(318r)				r												
I10(320p)						p										
I10(322r)								r								
I10(323a)									a							
I10(324f)										f						
I10(325v)											v					
I10(326t)												t				
I10(327i)													i			
I10(325v)				R	G	P	G	R	A	F	v	T	I			
I10(325i)											i					
I10(325l)											l					
I10(325a)											a					
I10(325y)											y					
I10(325f)											f					
I10(325h)											h					
I10(325t)											t					

*Sequences of substituted peptides are derived from and aligned with the sequence of P18-I10, an immunodominant epitope of HIV-1 gp160 envelope glycoprotein of the IIIB strain for the H-2D^d-restricted murine CTL. In these peptides, L-amino acids are expressed as capital letters and corresponding D-amino acids are expressed as small letters.

supplemented with 2 mM L-glutamine, 50 μM 2-ME, 100 U/ml penicillin, 100 μg/ml streptomycin, 10% heat-inactivated FCS, and 10% Rat T-STIM (Collaborative Biomedical Products, Bedford, MA). To establish CTL lines, the generated CTLs were maintained by biweekly stimulation with the mitomycin C-treated I10(325v)-pulsed Neo and were termed LINE-IIIB(325D) cells. CTL clones were established from bulk CTL lines using a limiting dilution technique in 96-well U-bottomed microplates, as described previously (15).

CTL assay

The cytolytic activity of the CTL lines and clones was measured, as previously described (27), using a standard 5-h ^{51}Cr-release assay with various ^{51}Cr-labeled targets, as indicated in the figure legends.

Flow cytometric analysis

Flow cytometric analysis was performed to determine the surface molecule expression of the established CTL lines and clones using a FACScan analyzer (Becton Dickinson Immunochemical Systems, Mountain View, CA). We harvested 5×10^5 cells, washed them twice with serum-free RPMI 1640, and then pelleted them. Fluorescein isothiocyanate-conjugated monoclonal antibodies were added to pellets, and they were then incubated for 30 min at 4°C. Then, the cells were washed three times and resuspended with phosphate-buffered saline (PBS) containing 0.1% bovine serum albumin and 0.1% sodium azide. Dead cells were gated out by forward and side scatter based on propidium iodide uptake. Ten thousand events were acquired for each sample and analyzed using Cell Quest software (Becton Dickinson, Franklin Lakes, NJ).

mRNA extraction, reverse transcription, and PCR amplification

Poly(A) tail-bearing mRNA was isolated from CTL clones using the Fast Track mRNA Isolation Kit (Invitrogen, Carlsbad, CA) according to the manufacturer's instructions. Reverse transcription and PCR amplification of purified mRNA were performed with a GeneAmp RNA PCR Kit (PE Biosystems, Foster City, CA). For the synthesis of T-cell receptor Vβ-specific cDNA, Vβ7-specific primer (ACATCCCTAAAGGATACAGGG) and Vβ8-specific primer (ATATCCCTGATGGGTACAAGG) were used in conjunction with Cβ primer (CCGATGGGAGCACACGAACCCTTAAG). For the synthesis of T-cell receptor Vα-specific cDNA, Vα2-specific primer (AGCAATTCTGAACTGCAGTTA), Vα3-specific primer (CAGCCCGATGCTCGCGTCACT), and Vα16-specific primer (ATGGACTGTGTGTATGAAAC) were used in conjunction with Cα primer (ACTGGACCACAGCCTCAGCGTC).

DNA sequence analysis

PCR products were separated by electrophoresis on a 1% of agarose gel and sliced bands were purified by EASYTRAP glass powder (Takara Bio., Siga, Japan). We then analyzed the purified DNA by a direct-sequence technique, using the ABI PRISM Big Dye Terminator Cycle Sequencing FS Ready Reaction Kit (PE Biosystems), and we analyzed the sequences on the ABI PRISM 377XL DNA Sequencing System (PE Biosystems).

Molecular modeling

Because the actual 3D TCR structures for both Vβ7 and Vβ8.3 were unknown, we carried out comparative and homology modeling to elucidate the spatial relation between TCRβ (Vβ7 or Vβ8.3) and P18-I10 or I10(325v). Comparative modeling predicts the 3D structure of a given protein sequence (target) primarily on the basis of its alignment to one or more proteins of a known 3D structure (templates). It is usually difficult to accurately determine the 3D structure from a protein sequence by theoretical procedures. However, because the 3D TCRβ structure consists of a sandwich comprising a four-stranded antiparallel β-sheet and a three-stranded antiparallel β-sheet that are linked by a disulfide bond, and because the core portion was tightly bound by a hydrogen bond, the 3D structure of the TCRβ, especially the core portion, could be reliably predicted.

Following the above procedure, the so-called threading or 3D template-matching method (28) could be implemented to select templates. For this procedure, we used LIBRA (29) (http://www.ddbj.nig.ac.jp/search/libra_i-e.html) software in which compatible structures of a target sequence are sought from the structural library chosen from the Protein Data Bank (PDB), and the target sequence and 3D profile are aligned by simple dynamic programming. According to the alignment, sequence remounts on the structure and its fitness are evaluated by the pseudoenergy potential. The scores are then sorted from the best-matched templates and shown along with their alignments. Based on the obtained alignments between the template and the target Vβ sequence, a 3D model is calculated by the MODELLER software (30–33), by which five 3D models were obtained from five templates used.

To examine the interaction between the calculated TCR and P18-I10, TCR/peptide/class I MHC complex (PDB code 1kj2) was used for two reasons. First, the 3D structure of the MHC part of 1kj2 is almost identical to that of MHC used in our experiment, which is also resolved (code 1bii) and shows a H-2D^d class I MHC molecule presenting the HIV-derived peptide

P18-I10 (RGPGRAFVTI) (34). The amino acid sequence identity between 1kj2 and 1bii is ~90%. Second, 1kj2 is a TCR/peptide/MHC complex (5), whereas 1bii is only a peptide/MHC complex. In our 3D models, Vβ7 or Vβ8.3 was fitted to the TCRβ position in 1kj2 and was drawn by Mol Feat software (FiatLux, Tokyo, Japan).

Quantum chemical calculation

To study the effect of electric charge on the TCR recognition response, we calculated both the electronic state of P18-I10 and any changes therein based on a single amino acid substitution (325V with 325T) within the P18-I10 using the PM5 molecular orbital method (MOPAC2002) (35). In this calculation, hydrogen atoms were first added to the PDB 3D structures, and then the net charges of all atoms in them were obtained, with the PDB 3D structure being maintained.

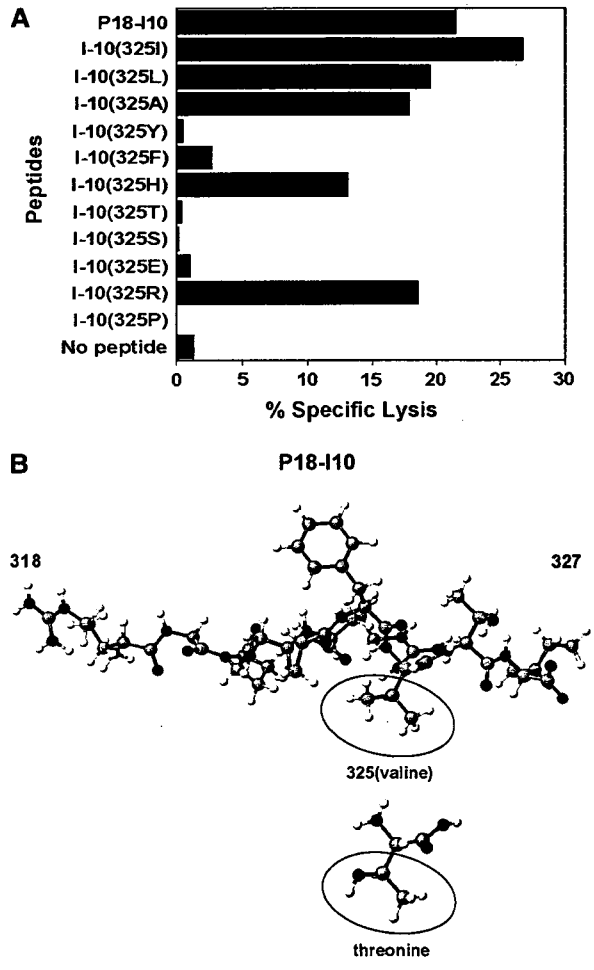

FIGURE 1 Effect of a single amino acid substitution at position 325 within P18-I10 on LINE-IIIB recognition. (*A*) Ten thousand of P18-I10-specific CTL line (LINE-IIIB cells) were added to 5000 ^{51}Cr-labeled BALB/c.3T3 fibroblast target cells in the presence of 3 μM of the substituted peptides at position 325 within P18IIIB, as shown in Table 1. Standard errors of the means of triplicate cultures were <5% of the mean in each case. Results are representative of three independent experiments. (*B*) Ball-and-stick model of peptide P18-I10. The amino acid side chain containing the valine (V) at position 325 within P18-I10 and threonine (T) are shown in the circle. Carbon, oxygen, nitrogen, and hydrogen are shown in gray, red, blue, and white, respectively.

RESULTS

Effect of a single amino acid substitution at position 325 within P18-I10 on LINE-IIIB recognition

First, to see the effect of a single amino acid substitution at position 325 where epitope specificity for LINE-IIIB recognition is determined, a series of P18-I10-derived peptides shown in Table 1 have been synthesized. Similar to our previous findings (10), we confirmed that LINE-IIIB cross-reacted with an aliphatic residue, such as I, L, or A at position 325, in addition to reacting with the original residue V. Moreover, LINE-IIIB cross-reacted with positively charged residues such as R and H but not with the negatively charged E or the uncharged T, S, or P at position 325 (Fig. 1 *A*). Here, we should focus on the case of T, because the 3D structure of the side chain of T is very similar to that of V. When only one carbon atom of the side chain of V is exchanged for one oxygen atom (Fig. 1 *B*; *red*), the amino acid becomes T, except for the hydrogen atoms. According to the quantum chemical calculation using Hamiltonian PM5, the net charge of the carbon atom in V was about $-0.3e$, whereas that of the oxygen atom in T is about $-0.4e$; e represents the elementary charge. This may be the reason why the recognition of V at position 325 by LINE-IIIB was dramatically changed by substitution with T. These results indicate that the charges of the amino acids within the epitope may affect the interaction between TCRs and peptide/MHC complexes.

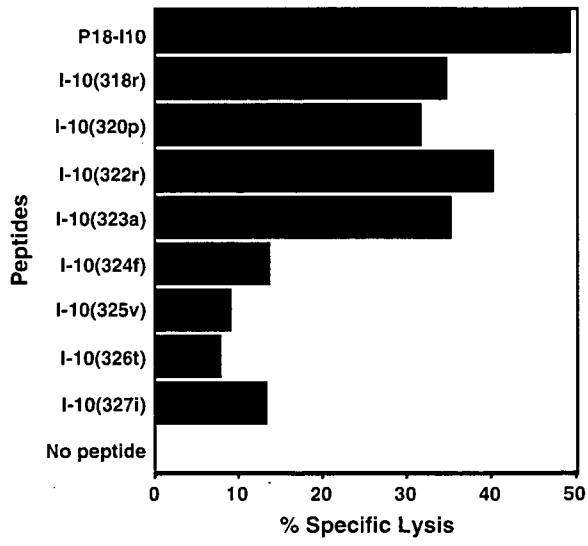

FIGURE 2 Effect of a single amino acid substitution with D-amino acid within an epitope peptide, P18-I10, on LINE-IIIB recognition. Ten thousand LINE-IIIB cells were added to 5000 ^{51}Cr-labeled BALB/c.3T3 fibroblast target cells in the presence of 3 μM of the substituted peptides with a single amino acid substitution by D-amino acid at each corresponding site (represented by lower-case letters in Table 1). Standard errors of the means of triplicate cultures were <5% of the mean in each case. Each experiment was performed at least three times.